Drivers for Atlantic-origin waters abutting Greenland

Laura C. Gillard[1], Xianmin Hu[1,2], Paul G. Myers[1], Mads H. Ribergaard[3], and Craig M. Lee[4]

[1]Department of Earth and Atmospheric Sciences, University of Alberta, Edmonton, Alberta, Canada
[2]Bedford Institute of Oceanography, Dartmouth, Nova Scotia, Canada
[3]Danish Meterological Institute, Copenhagen, Denmark
[4]Applied Physics Laboratory, University of Washington, Seattle, Washington, United States of America

Correspondence: Laura C. Gillard (gillard2@ualberta.ca)

Abstract.

The oceanic heat available in Greenland's troughs is dependent on the geographic location of the trough, the water origin, and how the water is impacted by local processes along the pathway to the trough. This study investigates the mechanisms that bring warm water to the shelf and into the troughs abutting the Greenland Ice Sheet (GrIS). Warm water that is exchanged
5 from the trough into the fjord may influence the melt on the marine terminating glaciers. Regional ocean model experiments showed that warm Irminger water can extend far north into Baffin Bay, reaching as north as Melville Bay troughs. Melville Bay troughs experienced warming following 2009. An increase in ocean heat in these troughs may drive a retreat of the GrIS. In 2004 to 2006, model experiments captured an increase in onshore heat flux in the Disko Bay trough, coinciding with the observed timing of the disintegration of Jakobshavn Isbrae's floating tongue and observed ocean heat increase in Disko Bay.
10 Seasonality of the maximum onshore heat flux differs due to distance away from the Irminger Sea. Ocean temperatures near the north-west coast and south-east coast respond differently to changes in meltwater from Greenland and high frequency atmospheric phenomena. With a doubling of the GrIS meltwater, Baffin Bay troughs transported ~ 40 % more heat. The lack of presence of storms resulted in an increase in heat flux (~ 20 %) through Helheim glacier's trough. These results demonstrate the regional variability of onshore heat transport through troughs and its potential implications to the GrIS.

15 *Copyright statement.* TEXT

1 Introduction

The Greenland Ice Sheet (GrIS), with the second largest storage of fresh ice on earth, has a glaciated cover of 1.81 million km^2 (Rastner et al., 2012). With the volume of ice reaching 2.96 million km^3, if the entire ice sheet were to melt, the sea level equivalent (SLE) would be ~ 7 m (Bamber et al., 2013). The GrIS recorded a maximum mass loss in 2012 with values reaching
20 -446 ± 114 Gt yr^{-1}, a SLE of $\sim 1.2 \pm 0.3$ mm yr^{-1}, and has varied around ~ 1 mm yr^{-1} SLE since (van den Broeke et al., 2016). Analysis of the the GrIS's mass loss and equivalent sea level rise (SLR) has shown that the GrIS has recently become a major source of global mean SLR (van den Broeke et al., 2016).

Meltwater originating off the south-west coast of the GrIS has been shown to circulate into the interior of the Labrador Sea (Gillard et al., 2016; Boning et al., 2016; Luo et al., 2016; Dukhovskoy et al., 2016). The Labrador Sea convection region is sensitive to changes in buoyancy, a balance between heat loss and freshwater input (Aagaard and Carmack, 1989; Straneo, 2006; Weijer et al., 2012). Thus, an increase of the accumulation of meltwaters in the Labrador Sea may affect and slow down

5   deep convection (Weijer et al., 2012; Boning et al., 2016). A weakening of the deep water formation may impact the Atlantic Meridional Overturning Circulation (AMOC), influencing how the earth distributes heat, impacting sea ice production and concentration of dissolved gases such as oxygen and carbon dioxide, and altering ecosystems (Weijer et al., 2012; Swingedouw et al., 2014; Boning et al., 2016; Arrigo et al., 2017).

Numerous studies have focused on the causation for the increase in mass loss from the GrIS, such as atmospheric warming

10   (Box et al., 2009) and synoptic wind patterns (Christoffersen et al., 2011). The annual mass balance of the GrIS has been persistently negative since the rapid retreat of marine terminating glaciers began in 1995 (van den Broeke et al., 2016).

There are approximately 900 marine terminating glaciers on the GrIS (Rastner et al., 2012) which drain ~ 88 % of the ice sheet (Rignot and Mouginot, 2012). Therefore, it is this type of glacier that has the greatest control over the fate of the ice sheet. Past studies have concluded that the influences affecting the dynamics of marine terminating glaciers include glacier

15   surface thinning (Csatho et al., 2014), glacier fjord geometry (Porter et al., 2014; Fenty et al., 2016; Rignot et al., 2016a; Williams et al., 2017; Felikson et al., 2017), state of the ice melange (Moon et al., 2015), subglacial discharge (Jenkins, 2011; Bartholomaus et al., 2016), and ocean temperature changes (Holland et al., 2008; Myers and Ribergaard, 2013; Straneo and Heimbach, 2013; Rignot et al., 2016b; Cai et al., 2017; Wood et al., 2018). Wood et al. (2018) showed that ocean warming at intermediate depths, below 200 m, has the potential to increase ocean induced undercutting.

20   The fluctuation of heat content in the North Atlantic Subpolar Gyre (NASPG) may have been the cause of ocean warming in fjords of marine terminating glaciers (Holland et al., 2008; Myers and Ribergaard, 2013; Straneo and Heimbach, 2013). The NASPG contains a branch that travels northward across the North Atlantic Ocean to the West European Basins (Fig. 1). Here, a branch travel westward, forming the Irminger Current circulating along Reykjanes Ridge. The Atlantic water that remains in the Irminger Current carries relatively warm and saline waters along the south-east coast of Greenland, while Polar

25   waters from the Arctic Ocean and Greenland meltwaters from the East Greenland Current (EGC) and East Greenland Coastal Current merge to create a (mixed and modified) relative cold and low-saline current (Bacon et al., 2014). This current forms the West Greenland Current (WGC) near Cape Farewell. The WGC separates into two branches: one travels northward along the west coast of Greenland into Baffin Bay bringing with it both less saline, cold Polar water and relatively warm, saline, modified Atlantic water, and the second, warmer and more saline branch joins the southward flowing Baffin Island Current

30   at Davis Strait (Fratantoni and Pickart, 2007; Myers et al., 2009). A portion of the NASPG branches off northward through the Iceland–Scotland ridge, which separates the Norwegian Sea from the North Atlantic Ocean, as the Norwegian Atlantic Current (NwAC) (Beszczynska-Möller et al., 2012). Instead of recirculating in the Fram Strait, a part of the NwAC can enter Barents Sea, south of Spitzbergen or north through Fram Strait (Beszczynska-Möller et al., 2012). A large volume of water that travels through Fram Strait may recirculate directly in the strait and return south to the Nordic Seas (Karcher et al., 2011;

35   Beszczynska-Möller et al., 2012). Another water source in Fram Strait may have originated from the Pacific Ocean (Aksenov

et al., 2010; Hu and Myers, 2013). Pacific Water in Fram Strait is mainly the water mass entering the Arctic Ocean via the Bering Strait and delivered through the Transpolar route (Hu and Myers, 2013).

Along the shelf break of Greenland, transverse troughs extend across the coast of Greenland supplying warm water through to the mouths of fjords. Then depending on the structure of the water mass at the mouth of the fjord and the height of the fjord's sills, warm waters can access the marine terminating glaciers and accelerating their mass loss (Straneo et al., 2012; Gladish et al., 2015b; Cai et al., 2017). If the warm waters from the NASPG can reach these transverse troughs, changes in heat content of the NASPG may influence the state of marine terminating glaciers on the GrIS.

This study investigates the following questions: how is heat flux through the troughs affected by ocean model resolution? What is the mean and variability of heat flux through the troughs around Greenland? What are the processes that drive the variability of flux?

2 Methods

2.1 Model description

A general circulation coupled ocean–sea ice model is utilized in this study. The fundamental modelling framework used is the Nucleus for European Modelling of the Ocean (NEMO) version 3.4 (Madec, 2008). The ocean component is based on Ocean Parallelise (OPA) and is used for the ocean dynamics and thermodynamics. For sea ice dynamics and thermodynamics, Louvain la Neuve Ice Model (LIM2) is used (Fichefet and Morales Maqueda, 1997). The regional domain for the coupled ocean–sea ice model covered the Arctic and Northern Hemisphere Atlantic Oceans (ANHA), with two open boundaries: one at the Bering Strait and the other at the latitude of $20°$ S. All simulations start from January 2002, and are integrated to December 2016.

Initial and monthly open boundary conditions (temperature, salinity, horizontal velocities, and sea surface height) are derived from the $^1/_4^°$ Global Ocean Reanalyses and Simulations (GLORYS2V3) product (Ferry et al., 2008). The surface atmospheric forcing fields (10 m surface wind, two metre air temperature and humidity, downward shortwave and longwave radiation, and total precipitation) with a temporal resolution of one hour and spatial resolution of 33 km, are from the Canadian Meteorological Centres Global Deterministic Prediction System Reforecasts (CGRF), provided by Environment and Climate Change Canada (Smith et al., 2014). The first two years of the model output are regarded as the adjustment from the initial GLORYS2V3 fields, which have already had over 10 years to evolve. Figure. 2 shows the monthly summation of total kinetic energy (TKE) in all layers of Baffin Bay, for two configurations, that will be discussed in detail in the next section, LowResControl and HighRes (Fig. 2a,b). The TKE is low at the model start (January 2002) and increases abrupt after 2004 for the LowResControl configuration. For the HighRes, the TKE is fairly comparable for all other years having more than a magnitude higher values compared to the LowResControl. Figure 2 suggests that the spin up of the large scale Baffin Bay circulation from the initial conditions takes one to two years, although it would take much longer for the deep layer and the interannual variation is not considered. Thus, only five–day averaged model output from 2004 to 2016 are analyzed in this study.

2.2 Sensitivity experiment set-up

2.2.1 Control experiment

The ANHA horizontal mesh grid is extracted from a global tripolar grid, ORCA (Barnier et al., 2007), at a $^1/_4{}^\circ$ resolution (hereafter referred to as LowResControl for low resolution) with a resolution ranging from ~ 11 km to ~ 15 km around Greenland. In the vertical, the LowResControl configuration uses the geopotential or z–level coordinate with a total of 50 levels. The layer thickness increases from 1.05 m at the surface level to 453.1 m in the last level (at a depth of 5727.92 m). Vertical high resolution is applied to the upper ocean, i.e., 22 levels for the top 100 m. Partial step (Bernard et al., 2006) is also enabled to better represent the sea floor. Bathymetry in LowResControl is taken from the existing global ORCA025 bathymetry (MEOM, 2013), which is based on a global relief model (ETOPO1) (Amante and Eakins, 2009) and a gridded bathymetric data set (GEBCO1) (BODC, 2008) with modifications (Barnier et al., 2007).

This study will focus on the relatively large scale processes outside of the fjords (as fjords are not resolved in this configuration) with an assumption that meltwater will reach the ocean surface once out of the fjord (Fig. 3). This assumption defines how Greenland discharge is added in the model, injected at the surface level then mixed into a 10 m thick layer. This approach is common in the present generation of ocean models at this horizontal scale, such as in Castro de la Guardia et al. (2015) and Dukhovskoy et al. (2016). Observations (Beaird et al., 2017, 2018) have shown that freshwater may not only be at the surface but be mixed and entrained with ambient waters and find a neutral buoyancy at depth. Therefore this stratification assumption in this model may be misrepresenting plume dynamics that occur in fjords and may need to be rethought in future studies.

The LowResControl simulation uses two interannual monthly runoff sources. Greenland's freshwater flux (tundra and icesheet runoff) is provided by Bamber et al. (2012) for 2002 to 2010, and 2010 runoff is repeated for the last 6 years of this study. Runoff in the rest of the model domain (not including Greenland) is provided by Dai et al. (2009). The model used in this study does not have an iceberg module and so only the icesheet and tundra runoff is included of Greenland's freshwater flux (~ 46 % of the total).

2.2.2 Changes in resolution

How is heat flux through the troughs affected by ocean model resolution? A $^1/_{12}{}^\circ$ horizontal mesh grid is extracted from a global tripolar grid, ORCA (Barnier et al., 2007) (hereafter referred to as HighRes for high resolution) with a resolution ranging from ~ 3.5 km to ~ 5 km around Greenland. The vertical resolution remains identical to the LowRes, however the HighRes bathymetry is built using a different approach. The bathymetry is generated by using ETOPO1 (Amante and Eakins, 2009) for the polar region, and the Global Predicted Bathymetry (Smith and Sandwell, 1997) from satellite altimetry and ship depth soundings for the rest of the domain. Therefore, given the different approach of the generated bathymetry, downscalling HighRes will not reduce to LowRes. The HighRes configuration provides model fields at a finer scale that is not always visible in LowRes. This provides the potential for a better simulation of warm ocean currents travelling towards the GrIS via a better representation of deep troughs. In addition, model resolution also plays a role in simulating ocean mixing and mesoscale features, such as eddies, that bring warm water towards the shelf through the trough along the GrIS. Note that, even in the

$^1/_{12}^{\circ}$ resolution referred to as HighRes in this study, the majority of the fjords are still not resolved. HighRes has the same runoff and Greenland's freshwater flux setup as LowResControl. Given the numerical cost of the HighRes, LowResControl is utilized for the sensitivity experiments.

2.2.3 Enhanced Greenland discharge experiment

5   How can changing Greenland's freshwater flux impact the heat flux troughs around Greenland? As Castro de la Guardia et al. (2015) showed, enhanced Greenland melt can change nearby ocean circulation, e.g., Baffin Bay. Here we conduct a pair of sensitivity experiments (LowResControl and LowResDoubleMelt) with more realistic spatial distribution and temporal varying Greenland freshwater flux to quantify the impact on warm waters flowing towards the marine terminating glaciers through troughs.

10   LowResControl under-represents the total of Greenland's freshwater flux. Therefore, LowResDoubleMelt, takes into account the solid mass discharge. LowResDoubleMelt has the identical setup as LowResControl, ~~expect~~ for Greenland's freshwater flux. It is important to note that the entire solid discharge in LowResDoubleMelt is transformed into the liquid component (i.e., treated the same as the runoff). In addition, the ocean does not affect GrIS melting as the melting is prescribed and non-interactive. This results in roughly twice as much freshwater flux (hereafter called meltwater) (100 % Greenland's freshwater

15 flux, broken down by ~ 46 % runoff and total iceberg discharge ~ 54 %) in LowResDoubleMelt compared to LowResControl (roughly 46 % of Greenland's freshwater flux, only including runoff). Therefore, the total meltwater added to LowResDoubleMelt had been rouglhy doubled, and actually has a more realistic amount of meltwater than LowResControl. For this study, a comparison of the GrIS meltwater is made to demonstrate the ocean model's sensitivity to increased GrIS melt. How will ocean temperatures in troughs that terminate into Baffin Bay be impacted by an increase in GrIS melt?

2.2.4 High frequency atmospheric event experiment

Previous studies (Holdsworth and Myers, 2015; Garcia-Quintana et al., 2019), have shown that high frequency atmospheric phenomena, such as storms, barrier winds, fronts, and topographic jets, play an important role in the ocean processes (e.g., deep convection in the Labrador Sea) in the study area. Do they also influence warm water brought towards the GrIS? Until this study, this has not yet been examined.

25   We use the Kolmogorov–Zurbenko (KZ) filter method (Zurbenko et al., 1996) as Eskridge et al. (1997) has shown that this filter has the same level of accuracy as the wavelet transformation method, however is much easier to use. The KZ filter is based on an iterative moving average that removes high frequency variations. We apply the moving average over a length of 10 days with one iteration as Garcia-Quintana et al. (2019) has done. Therefore, the removal of atmospheric variability ~~(such as temperature and wind speeds) that~~ persisted for ~~a length of~~ 10 days or less from the atmospheric forcing was done to drive

30 a sensitivity simulation, called LowResNoStorms. LowResNoStorms has the identical setup as LowResControl, except for the KZ filter applied in the wind and air temperature fields (Zurbenko et al., 1996; Eskridge et al., 1997). For more information regarding the methodology of the KZ filtering, please see Zurbenko et al. (1996); Eskridge et al. (1997). A complete list of simulations used in this study is given in Table 1.

2.3 Mean flow and its fluctuation

To evaluate the ocean's heat that reaches onto the shelf and into the troughs, heat fluxes are calculated at six sections along the coast of Greenland (across one trough per section, as shown in purple and tan, respectively, in Fig. 1). Section names and their associated trough names are seen in Fig. 1. To calculate the fluctuation of the heat flux, the five day average model output of both temperature (T) and velocity (U) normal to the section are treated as the full current. A moving averaged Eq. (1) was applied by ~~taking the~~ average of five model outputs (25 days) centered on a particular output (n) by taking outputs from two previous (($n-2$) and ($n-1$)), the centered (n), and two future (($n+1$) and ($n+2$)). The mean of the temperature and velocity normal to the section ($\overline{T}$,$\overline{U}$) can be taken over a longer period (25 days). The mean values were then subtracted from the full current to get the fluctuation component of the heat flux in Eq. (2). Given Eq. (2), ρ_0 is the reference density, Cp is the specific heat capacity of sea water, x is the length of the section, $H(z,x)$ is the water depth along the section, $T(t,z,x)$ is the temperature, and $U(t,z,x)$ is the velocity normal to the section.

$$(\overline{U},\overline{T}) = \frac{1}{5}\sum_{n-2}^{n+2}(U,T)_{T}$$

(1)

$$HeatFlux_{eddy}(t) = \rho_0 Cp \int_0^x \int_0^{H(x)} U(t,z,x)T(t,z,x) - \overline{U}(t,z,x)\overline{T}(t,z,x)dzdx$$

(2)

To see the importance of the fluctuation component of the flow around Greenland, the eddy kinetic energy (EKE) was calculated using the five day averaged model outputs of velocity in the zonal (u) and the meridional (v) components. The EKE was calculated using Eq. (3). Then the annual EKE average over the period of 2004 to 2016 were calculated.

$$EKE = \frac{(\overline{u^2} - \overline{u}^2) + (\overline{v^2} - \overline{v}^2)}{2}$$

(3)

2.4 Model evaluation

In order to continue with this study, a comparison was done to make sure that the model behaves similar to observations. A comparison of the model behavior against observations was done for West Greenland. The water mass structure at Fylla Bank is compared to observations from Ribergaard (2014). This section is chosen, as the WGC branches shortly after ~~it has~~ passed Fylla Bank, with a portion moving westward and joining the Labrador Current while the other portion continues north through Davis Strait. The Fylla Bank section is shown with magenta in Fig. 1 (red in Fig. 1 in Ribergaard (2014)). The observed temperature and salinity for June 14th, 2013 (Fig 31 in Ribergaard (2014)) is compared to the modeled averages for June 2013 (Fig. 4). LowResControl (Fig. 4a.) has a similar water mass structure as observations. There is cooler water at the surface with a thickness of 50 m offshore and about 100 m, just off the west side of the bank (kilometre marker 45), with warmer water (greater than $3°C$) below 100 m depth. The cold water layer in the LowResControl is slightly saltier with the depth of the

modelled 34.2 isohaline similar to that of the observed 34 isohaline (Fig. 31 in Ribergaard (2014)). For the HighRes, the cold surface layer is thicker (Fig. 4b.) than in observations, where the $2\,^{\circ}C$ layer (contour in magenta) extends to about 100 m depth off the west side of Fylla Bank at kilometre marker 45. Similar to observations the $4\,^{\circ}C$ and warmer water mass starts below 200 m and slopes upwards towards the west. At a depth of ~ 400 m the HighRes is warmer than observations by $\sim 1\,^{\circ}C$. Overall, the modelled water mass structure compares well with the observations but with minor offsets in temperature and salinity. The model has a shallow fresh and colder surface layer in the west portion of the section, and deepens towards Fylla Bank. Finally, the HighRes configuration has a much stronger and better represented thermocline compared to the LowResControl configuration

Moving northward to Davis Strait, a primary gateway for meltwater and heat exchange between Baffin Bay and the North Atlantic Ocean. A comparison was done with LowResControl and HighRes to the Curry et al. (2014) moored array (see Fig. 2 in Curry et al. (2014)). The monthly modelled temperature averaged over 2004 – 2010 at Davis Strait (Fig. 5 and Fig. 6) is compared to the mooring observations (Curry et al. 2014, their Fig. 3(c)). July through to September LowResControl (Fig. 5) captures the same structure of the West Greenland Slow Water (WGSW) and West Greenland Irminger Water (WGIW) as in the Curry et al. (2014) study. From March to June LowResControl shows WGIW and WGSW cooler ($\sim 3\,^{\circ}C$) by about a degree than that of the observations ($\sim 4\,^{\circ}C$). LowResControl also has a tongue of relatively warm water from the WGIW protruding into the interior of Davis Strait at $\sim 200\ km$ and $\sim 200\ m$ depth. For the HighRes (Fig. 6), the structure is similar to that of LowResControl, with the protruding tongue at $\sim 200\ km$ and $\sim 200\ m$ depth. HighRes also has a similar structure to the observations for the WGSW from July to October. Note that compared to observation, the WGSW and WGIW seems to be about $1\,^{\circ}C$ warmer.

The LowResControl and HighRes volume transport from September 2004 to September 2013 is able to satisfactorily represent the observations from a mooring array at Davis Strait (e.g. Curry et al. (2011, 2014)) (Fig. 7). Positive values indicates southward volume fluxes through Davis Strait, and negative values indicates the waters move northward. However, the simulations underestimate the high frequency peaks of transport from the observations (values surpassing 6 Sv in some cases). Lack of tides in the model may explain why there is less fluctuation of transport compared to observations. The mean volume flux based on the Davis Strait moorings (Curry et al., 2011, 2014), calculated over the time period of Sept 21, 2004 to Sept 30, 2013, is 1.6 Sv. Over the same time period, the model transports are 1.2 Sv for LowResControl, with a correlation of 0.54, and 1.0 Sv for HighRes with a correlation of 0.49. Yet many features, such a the reduction in transport at the end of 2010, are well simulated.

2.5   Study area

This study focuses on six sections around Greenland (Fig. 1) with marine terminating glaciers and deep bathymetric features. In Fig. 8, the six sections are drawn (seen in light purple on the map inset 1). HighRes model bathymetry is in grey and each section runs north to south on the x–axis starting at the left hand side of the figure indicated by the zero kilometre marker. The rest of this section will compare the six sections and discuss how observed bathymetry from other studies compares to the HighRes model bathymetry (Fig. 8).

In north-west Greenland, Kong Oscar is the fastest marine terminating glacier, terminating into Melville Bay (Rignot and Kanagaratnam, 2006; Rignot and Mouginot, 2012). Twenty percent of the GrIS drainage volume is directed along glaciers that feed into Melville Bay, amounting to a discharge of ~ 80 km^3 yr^{-1} (Rignot and Kanagaratnam, 2006). Located in north-east Baffin Bay (Fig. 1), Melville Bay holds the widest and deepest Greenland cross shelf troughs. This system consists of three troughs: the North, Centre, and South Melville Bay Troughs (MVBTs: MVBNT, MVBCT, and MVBST). The MVBTs are 170 to 320 km long, 45 to 120 km wide and reach depths between 740 m to 1100 m with shallow banks (around 100 m below sea level) called inter–trough banks (Slabon et al., 2016; Morlighem et al., 2017). The HighRes bathymetry (seen in Fig. 8a) is relatively shallow compared to the observations discussed. MVBNT is located at the kilometre markers 10 km to 120 km, MVBCT at 320 km to 450 km, and MVBST at 480 km to 580 km. The depths in the HighRes are about 400 m for MVBNT, and reaching almost 700 m depth for MVBCT and MVBST.

Further south, on the west coast of Greenland, Jakobshavn Isbrae (JI) terminates into Disko Bay. The rapid retreat and disintegration of JI's floating ice tongue has been attributed to an increase in heat content, deep bathymetry, and NASPG warming (Holland et al., 2008; Myers and Ribergaard, 2013; Gladish et al., 2015a; An et al., 2017). Recent slowing down of JI's acceleration has been attributed to the glacier reaching a higher bed, high amounts of freshwater from the Canadian Arctic, a weak WGC, or a cold Baffin Bay current flooding the West Greenland Shelf and cooling in the Labrador and Irminger Seas (Joughin et al., 2012; Gladish et al., 2015a; An et al., 2017; Khazendar et al., 2019). In HighRes, the section drawn for Disko Bay (Fig. 8b) shows two deep bathymetric features: the first trough, located at 100 km to 200 km, and the second trough at 380 km to 500 km, now called UT (Uummannaq Trough) and DBT (Disko Bay Trough), respectively. UT connects to Uummannaq Fjord and DBT connects into Disko Bay. Both UT and DBT reach depths of around 500 m, similar to observations found in (Hogan et al., 2016). In a more recent data set provided by BedMachineV3, UT similarly reaches approximately 500 m but DBT is much deeper, reaching depths of 900 m (Morlighem et al., 2017).

In the south-east region there are two major glaciers of interest: Helheim Glacier (HG) and Kangerlussuaq Glacier (KG). HG terminates at a depth of 700 m in Sermilik Fjord, which is approximately 900 m deep at the U shape mouth with the adjacent continental shelf, reaching depths of 350 m (Straneo et al., 2010; Morlighem et al., 2017). Temperature variability in Sermilik Fjord cannot be explained by local heating or surface fluxes. The temperature variability in the fjord is instead a result of the advection of warmer waters into the fjord, as warm waters are present on the shelf year round, peaking from July to September (Straneo et al., 2010). In HighRes, the section drawn for HG (Fig. 8c) shows four unique features. The first one at kilometre marker 25 km to about 100 km shows a slumping of bathymetry reaching about 250 m in depth. Moving further south there are three deep troughs. The first trough is located at 120 km to 180 km, reaching depths surpassing 500 m, and the second and third troughs, located at 190 km to 260 km and 350 km to 375 km, respectively, reach depths closer to 700 m. Features will be referred to as Slump, HGT1, HGT2, and HGT3.

In the BedMachineV3 data set, Kangerdlussuaq trough (KT) reaches depths closer to 800 m (Morlighem et al., 2017). Atlantic water occupies the deep waters of the KT and Kangerlussuaq Fjord (KF) (Azetsu-Scott and Tan, 1997). KF, similar to Sermilik Fjord has a deep open mouth, which could influence the Atlantic water transport that is observed there (Azetsu-Scott and Tan, 1997; Christoffersen et al., 2011; Inall et al., 2014). In HighRes, the section drawn for KT (Fig. 8d) is drawn over an

area with the maximum depth in the middle of the section, deeper than 600 m, at kilometre marker 175 km. The KT extends from 125 km to about 200 km.

In the north-east, Daugaard-Jensen Glacier terminates into Scoresby Sund and Nioghalvfjerdsbrae (79NG) terminates into the sound of Jøkelbugten. The BedMachineV3 shows depths of around 600 m (Morlighem et al., 2017). The HighRes section drawn for Scoresby Sund (Fig. 8e) is outside of the opening of the coastline, from north to south, connecting fjord waters to the open ocean. The bathymetry here is smoother with fewer carved features. Instead it shows a skewed U shape in this section. The maximum depth is reached at kilometre marker 120 km with a depth slightly greater than 500 m.

79NG has a floating ice tongue that abuts Hovgaard Ø, which divides the tongue into two sections (Wilson and Straneo, 2015). The most rapid melting occurs at the grounded (pinned) front, south of Hovgaard Ø, where the ice tongue is thickest and is exposed to deeper and warmer waters (Mayer et al., 2000; Seroussi et al., 2011; Wilson and Straneo, 2015). Schaffer et al. (2017) study showed that Atlantic Intermediate Water flows via bathymetric channels to the south of Hovgaard Ø at a pinned ice front, where there is a shorter pathway between the shelf and cavity, exposing the cavity to more shelf driven processes such as intermediary flows. The warm water is supplied from the warm water that resides in Norske Trough (NT) east of Hovgaard Ø (Fig. 1) (Wilson and Straneo, 2015). Some of the relatively fresh glacially modified water is exported to the continental shelf via Dijmphna Sund, north of the glacier (Wilson and Straneo, 2015). In the BedMachineV3, NT reaches depths close to 600 m (Morlighem et al., 2017). The HighRes section drawn for 79NG (Fig. 8f) is drawn from north to south. The HighRes bathymetry shows the deepest region exceeding depths of 300 m, though the majority of this section lies around 200 m.

3 Results and discussion

3.1 Onshore heat flux through coastal troughs

What is the significance of the deep troughs along Greenland's shelf to the supply of warm water to the fjords with marine terminating glaciers? A look at the onshore heat flux through these troughs will be shown using HighRes, as the benefits of a higher horizontal resolution have been shown. However, given the numerical costs of the HighRes, LowResControl is utilized for the sensitivity experiments that will be discussed later in this paper.

3.1.1 West coast: mean state

The section drawn for Melville Bay (Fig. 8a), located on the north-west coast of Greenland, shows three deep bathymetric troughs: the MVBNT, MVBCT, and MVBST (all troughs described in Sect. 2.5). At the north edge of all three troughs (kilometre marker 15 km, 330 km, and 500 km, for MVBNT, MVBCT, and MVBST, respectively) there is an offshore heat flux. At the south edge of all three troughs (kilometre marker 110 km, 450 km, and 560 km, for MVBNT, MVBCT, and MVBST, respectively) there is an onshore heat flux. However, MVBNT, the shallowest of them, has the weakest onshore heat flux, 0

TW except for short periods during 2010, 2012 and 2014. This identifies that the northward warm waters travelling along the west Greenland coast are influenced by bathymetry and are steered eastward along the trough towards the coast.

MVBNT, MVBCT, and MVBST transport increased between 2009 and 2010 and persisted in an anomalously high state for five years. For MVBNT there was little heat transfer before 2010 when the heat transport through to 2015 increased to 0.05 TW. At MVBCT, an increase of heat flux started at the end of 2009, and reached a relatively stable value of 0.1 TW through to the end of 2016. For the MVBST there was a more persistent interannual heat flux throughout the entire period, increasing from 0.1 TW to 0.2 TW starting at the end of 2009. An increase in warm water flux through troughs in northern regions of Greenland shelf starting in 2009 for MVBCT and 2010 for MVBNT and MVBST was also identified. A change from 0.1 TW is significant, as that increase in heat can potentially melt 300 tons of ice per second. Thus, an increase in ocean heat presence in these troughs may have driven more melt from the glaciers that terminate in Melville Bay.

The section drawn for Disko Bay (Fig. 8b), located on the west coast of Greenland, shows two deep troughs: UT and DBT. Both troughs experience an onshore heat flux at the south edge (kilometre marker about 180 km and 480 km, for UT and DBT, respectively) and an offshore heat flux at the north edge (kilometre marker 100 km to 120 km and 400 km to 420 km, for UT and DBT, respectively). In addition to modified Atlantic water travelling northward via the WGC, along the coast, this study shows that the ocean currents are influenced by the bathymetry and are steered eastward into the trough towards the coast.

HighRes was able to capture a relatively higher heat flux in UT and DBT in the early 2000s (2005 for UT and 2004 to 2007 for DBT). For UT there are specific events when the heat flux peaked up to ~ 0.3 TW, and at the end of 2005 there was a peak heat flux of about 0.1 TW and then through 2010 to 2012 there are variable pulses (0.1 TW) with maximum in the winter of 2010–2011 with a value of 0.2 TW. There is a consistent heat flux onshore in DBT from 2004 to end of 2007, and an increase in the heat flux (values showing 0.4 TW) reaching a maximum in 2010 and then decreasing back towards 0.35 TW afterwards. The increased heat flux in years of 2004 to 2006 coincide with the disintegration of the JI floating tongue, and within the period of observed oceanic heat increase Disko Bay (from 1997 to 2007) (Holland et al., 2008).

3.1.2 West coast: seasonal and interannual variation

The seasonality of the average onshore heat flux is shown in MVBCT (Fig. 9a). Late fall and early winter shows the maximum onshore heat flux with a peak in November. Through late winter to spring onshore heat flux is weakest, with the minimum in April. Years of 2004–2007, as indicated in a variety of blues, overall have less onshore heat flux. As time progresses, the onshore heat flux increases. 2011 and 2014 (as indicated in colours of pale green and orange) show the highest values of onshore heat flux, reaching maximums of about 13 TW and 11 TW respectively. Again this indicates that more heat has been received into MVBCT in more recent years. The lack of a summer peak at MVBCT, suggests seasonality is dominated by the subsurface warm layer. MVBCT heat flux seasonality seems to be dependent on both the seasonality of the volume flux and temperature (Fig. 9b and Fig. 9c), with a correlation of 0.92 and 0.93 (shown in Table 2).

Further south in DBT (Fig. 9d), fall and winter seasons have higher onshore heat flux. However, earlier years (2004 to 2005) show above average onshore heat flux in the summer. A maximum onshore heat flux was identified in July and August of 2004 and 2005 (reaching values around 7 TW to 10 TW). However in other years, June and July have lower values of heat flux

(hovering close to 0 TW). This peak in 2004 to 2006 is shown in DBT (Fig. 8b). In 2011 there is a spike of onshore heat flux in December, reaching over 10 TW, then decreased in January (Fig. 9d). For UT, in 2011, there was also a peak onshore heat flux (Fig. 8b).

Observations at Davis Strait see a temperature maximum in August through to November (Curry et al., 2011). The results here show DBT received onshore heat flux earlier in the season in the period of 2004 to 2006, around June and July, coinciding with warmer surface waters. As the years progressed in the model the timing of the maximum heat flux becomes later in the season, from September to January, coinciding with the peak in the Irminger Water (Fig. 9d). The August–December lag corresponds to the advection time from when the water was last near the surface in Irminger Sea. These results show an early arrival in warm waters occurred at the time when JI melted rapidly (Holland et al., 2008). This may therefore have been due to not only increase in ocean heat flux but perhaps an arrival of warm waters earlier in the melt season and stayed for a longer time. DBT heat flux seasonality is dependent on the seasonality of the temperature of the water mass and not the seasonality of the volume flux (Fig. 9f and Fig. 9e), with a correlation of 0.93 and 0.43 (shown in Table 2).

3.1.3   South-east coast: mean state

The section drawn for Helheim (Fig. 8c) located off the south-east coast of Greenland, shows four unique features, Slump, HGT1, HGT2, and HGT3. For this section, HGT1 through to HGT3, at the north edge of the troughs (kilometre marker 100 km, 200 km, and 350 km) there is an onshore heat flux, and an offshore heat flux at the south edge (kilometre marker 175 km, 225 km, and 355 km). This identifies that there must be southward flowing warm water travelling along the south-east coast of Greenland, potentially drawn in from Irminger Current, and the warm waters are again being bathymetrically steered westward along the trough towards the coast. Slump shows an off shelf heat flux, oscillating from 0 TW to $\sim$- 0.5TW, potentially associated with lots of transient mixing and eddies.

The section drawn for KT (Fig. 8d), highlights the extent of this trough. On the north portion of the section, from about 25 km to 100 km there is evidence of mixing of signals of on and off shelf. At the 150 km mark, throughout the years, there is a consistent onshore heat flux of greater than 0.1 TW and similar in magnitude is an offshore heat flux on the south edge of the trough. This trough appears to have the strongest onshore signal of the section. At the south portion of the section (from 225 km to 325 km) there is a lot of variability of on and offshore in space and time.

3.1.4   South-east coast: seasonal and interannual variation

For HGT2 (Fig. 9g), the period of August through to May has the weakest onshore heat flux. However, offshore heat flux occurs all year round making this location unique compared to all other regions. Observations from a fjord in south-east Greenland (Sermilik Fjord) showed that water properties and heat content vary significantly on synoptic timescales throughout non-summer months (Jackson et al., 2014). Looking at HGT2 (Fig. 9g), from October to March there was large variability in the magnitude and direction of the heat flux, a period with an increase in average temperature (Fig. 9i).

Seasonality of HGT2 heat flux is related similarly to the seasonality of the volume flux (correlation of 0.91)(Fig. 9h), rather than the temperature (correlation of -0.25) (Fig. 9i) as shown in Table 2. At KT (Fig. 9j), a peak of onshore heat flux occurs

after August for most years. Summer onshore heat peaks occur in 2004, 2005, 2015, and 2016. KT heat flux seasonality seems to be dependent on both the seasonality of the volume flux and temperature (Fig. 9k and Fig. 9l), with a correlation of 0.83 and 0.89 (shown in Table 2).

3.1.5 North-east coast: mean state

The section drawn for Scoresby Sund (Fig. 8e), shows Scoresby Sund Trough (SBST). It is again on the north edge of the maximum depth, at kilometre marker 110 km that there is a consistent signal for onshore heat flux of more than 0.025 TW. On the north edge of the kilometre marker 20 km to 30 km, there is variability in the offshore heat flux. The middle of the section is where the heat is coming towards the coast.

The section drawn for 79NG (Fig. 8f), located north-east of Greenland, is drawn from north to south. On the north side of the trough, at around 400 km there is a pattern for onshore heat flux at different periods within the time series, and also similar for 1000 km and 1100 km. This area's bathymetry is quite complex and the deeper regions such as kilometre marker, 40 km, and from 1000 km to 1100 km, has heat flux onshore. The onshore heat flux has a much smaller magnitude than any of the other sections, reaching its maximum value at about 0.04 TW.

3.1.6 North-east coast: seasonal and interannual variation

At SBST (Fig. 9m), onshore heat flux begins to increase in October and declines in April. Peak years include early 2005, then 2010 and 2011, with 2016 having a weaker onshore heat flux. A maximum of 10 TW is reached in 2005. SBST heat flux seasonality seems to not be solely dependent on either the seasonality of the volume flux or temperature flux alone (Fig. 9n and Fig. 9o). The heat flux shows a negative correlation of -0.73 for the volume flux and -0.76 for the average temperature (shown in Table 2).

At NT (Fig. 9p) the seasonality is not clear. A consistent growth in onshore heat flux occurs in August, with a minimum of heat flux in June. There is a lot of variability from 2004 to 2016, with maximum flux in 2004, 2005, and 2010 and strongest offshore heat flux occurring in January through May of 2015. From August to December, maximum onshore heat occurred in 2006, 2010, and 2014, with a maximum offshore heat flux in 2004, 2009 and 2007. From 2012 to 2016 there is a peak in February with a decline in March and April. The heat flux then increases steadily to a maximum in September and October, where it then declines again. Therefore, for this region, the seasonality has changed throughout the time of the study. NT heat flux seasonality is dependent on both the seasonality of the temperature (Fig. 9r) an the volume flux (Fig. 9q), with a correlation of 0.81 and -0.99 (shown in Table 2).

3.1.7 Summary of onshore heat flux through coastal troughs

Of these six regions, the region closest to Irminger Sea, HGT2, receive the highest heat flux in June to September. The two regions farther away from the NASPG on the west coast of Greenland (MVBCT and DBT), have warm water transported later due to the arrival of warm Irminger Water from the subduction area in the Irminger Sea. DBT has the largest onshore

ocean heat flux from July to December. Further north, a later arrival occurs at MVBCT (September through December). On the north-east coast of Greenland, warm water is received from the NwAC. The transport through the three troughs peak in onshore heat flux thusly: KT from August to November, followed by SBST from November to April and the NT peaked from September to January. Therefore, HGT2 could receive warm water first from the Irminger Sea, then the WGC reaches DBT then MVBCT and the NwAC reaches KT, followed by SBST and NT. For the WGC branch, Carroll et al. (2018) identified the warmest and saltiest Irminger water in Davis Strait during summer months, this would align with the timing of the arrival of warm waters in the troughs along the west coast of Greenland, as their is a lagged time when the warm water is shown in these troughs, in summer or fall. The seasonality of heat flux through these troughs seems to correspond with the volume flux (HGT2) or average temperature (DBT and NT), and even both components in some cases (MVBCT, KT). SBST had a negative correlation with both the volume flux and the average temperature, where there is less onshore heat flux in the summer months (July to October) there is more onshore volume flux and warmer ocean temperatures. Where in the winter months, there is more onshore heat flux, but more offshore volume flux and cooler ocean temperatures.

3.2   Contribution of the mean flow and its fluctuation

An ocean current can be broken down into two components, mean and fluctuation. Sect. 2.3 defines how the mean and fluctuation components are calculated (using Eq. (2)). Examining the mean and fluctuation components of the current will help identify what processes drives the heat flux through the troughs (Fig. 10). This section will compare LowResControl and HighRes.

For the west coast of Greenland, MVBCT and DBT show that the mean flow is crucial for bringing heat on the shelf (Fig. 10a and Fig. 10c). For MVBCT (Fig. 10b) the fluctuation component is negligible, approximately 0 TW with the mean component reaching a maximum of ∼ 13 TW in the HighRes. LowResControl total (mean and fluctuation) onshore heat flux correlates well with the HighRes with a value of 0.84 (Table 3). LowResControl transport is lower and reaches it's peak of approximately 7 TW at the end of 2012. From the end of 2005 the arrival of the heat flux occurs at the end of the year, consistent with Fig. 9a.

With DBT (Fig. 10d), the fluctuation component is less than the mean component. The maximum absolute value of the fluctuation heat flux is 1.3 TW and the maximum absolute value of the mean heat flux is 11 TW. Mean peaks occurred throughout the period with interannual variability, with a maximum in July and August in 2004 to 2007 and at the end of the year (November) in 2007 to 2010, 2013 and 2014 (in October). LowResControl total (mean and fluctuation) onshore heat flux does not have a strong correlation with the HighRes with a value of 0.54 (Table 3). The maximum onshore heat flux in HighRes, in 2004 and 2011 is 11 TW and 7 TW for LowResControl in 2004. The summation of yearly heat flux of MBVCT and DBT is 96 % higher in the HighRes than the LowResControl (Table 4). This maybe as seen in Section 2.4 (Fig.6), that the HighRes resolves about a $1\,°C$ warmer water mass at Davis Strait than compared to observations (Curry et al., 2014).

The south-east Greenland trough, HGT2, shows that the fluctuation component has transports between 0 TW to ∼ 4 TW in HighRes (∼ 2.5 TW in LowResControl) of onshore heat flux (Fig. 10f). The fluctuation is crucial for bringing heat onto the shelf especially for HighRes, as there is a large mean offshore heat flux through the study period (Fig. 10e). LowResControl

total (mean and fluctuation) onshore heat flux correlates well with the HighRes with a value of 0.77 (Table 3). For LowResControl the offshore heat flux ranges from -15 to 5 TW, where HighRes ranges from -30 to 0 TW . It is due to the mean velocity, normal to the section, that is driving the offshore heat exchange. The fluctuation component of the flow having an impact on the control of the oceanic heat is consistent with studies that have looked at strong wind events in this region bringing warm waters

5   to the coast (Christoffersen et al., 2011). How winds may impact the ocean heat flux will be discussed later in this section.

For KT, both the mean component and fluctuation component contribute to the onshore heat flux similarly in LowResControl and HighRes (Fig. 10g and Fig. 10h). There was variability with on and offshore pulses with the mean and fluctuation components, though the fluctuation is larger for HighRes than LowResControl. LowResControl onshore heat flux correlates well with the HighRes with a value of 0.71 (Table 3). For HighRes, the mean onshore heat flux reaches a maximum at the end

10   of 2004 and 2014 with values of approximately 14 TW, whereas LowResControl reaches about 7 TW in those years.

It is interesting to note the differences between HGT2 and KT, in HighRes, since they are located in close proximity to each other. The summation of yearly heat flux of HGT2 and KT is 4 % higher in the HighRes than the LowResControl (Table 4). Therefore, overall there is not a large change in HighRes vs LowResControl.

In the north-east at SBST (Fig. 10i) varying the resolution does not impact the mean onshore heat flux. LowResControl total

15   (mean and fluctuation) onshore heat flux correlates well with the HighRes with a value of 0.74 (Table 3).The fluctuation of the heat flux (Fig. 10j) has little contribution onshore for most of the study period, though there is an increase from $\sim \pm 2$ TW at the end of 2010 in HighRes. However, the mean onshore heat flux component is consistently higher for all simulations throughout the study period with peaks of ~ 10 TW in 2005. Peaks in the mean onshore heat flux occurs at the end of each year following into the beginning of the next year, consistent with the seasonality shown in Fig. 9m.

20   Further north at NT (Fig. 10k), LowResControl total (mean and fluctuation) correlations strongly with the HighRes with a value of 0.92 (Table 3). The mean component dominates over the fluctuation component for onshore heat flux. The mean component carries heat offshore as well with values reaching over -3 TW compared to ~ 0.5 TW onshore. The fluctuation component also contributes to carrying heat towards the shelf, with values reaching ~ 0.2 TW (Fig. 10l). The annual summation of onshore heat flux for the north-east coast (SBST and NT) is 9 % higher in the HighRes than the LowResControl (Table

25   4).

To see what is happening further off shelf, a section was drawn called NToff (Fig. 1). LowResControl total (mean and fluctuation) correlates strongly with the HighRes with a value of 0.92 (Table 3). There exists stronger onshore pulses of the mean heat flux (values reach 2 TW or up to as high at 4 TW) (Fig. 10m). Most onshore mean heat flux pulses occur at the end of each year though maximums of 4 TW occurred at the beginning of 2005, and end of 2011 into 2012. Like in NT, the

30   mean heat flux still contributes to the offshore component. There is not much different between the fluctuation of the heat flux between NT and NToff (Fig. 10n).

The percent difference of the annual summation of the onshore heat through NToff verus NT is 5.3 % and 6.5 % for HighRes an LowResControl, respectively. Therefore, NToff has more heat travelling through the section than NT. This may be to do the deepening off shelf allowing for warm waters to enter this region, and not closer to the shelf where the bathymetry shallows.

The correlation of the heat flux between the HighRes and LowResControl for most troughs is high (NT and NToff greater than 0.9, MVBCT greater than 0.8, and HGT, KT, and SBST greater than 0.7, see Table 3). The LowResControl compared well with observations (see Section 2.4). As running several high resolution experiments are computational expensive (such as HighRes) compared to lower resolution configurations (such as LowResControl), the LowResControl has been used for the sensitivity experiments (Section 3.3 and Section3.4).

3.3 Impact of enhanced Greenland meltwater

Through each section, the annual average onshore heat flux and the total onshore heat flux was calculated for the study period (2004 to 2016). A comparison between the experiments were made for each sector (west includes Melville Bay, Disko Bay, south-east includes Helheim and Kangerdlussuaq, north-east includes Scoresby Sund, 79NG sections) (Table 4). With double the meltwater, the west sector had a 37 % increase in onshore heat flux. It appears that this ~~mechanism~~ (increase of heat flux with an increase in meltwater) is not as strong or reproduced in any other sector (-5 % and 9 % for south-east and north-east sectors).

For Melville Bay in LowResControl (Fig. 11a), a warm core of water exists at depths 100 m to 400 m, with a maximum (kilometre marker 500 km) in MVBST reaching almost $2\,^{\circ}C$. In LowResDoubleMelt (Fig. 11b), the warm water core temperature increased and MVBST reaches temperatures closer to $3\,^{\circ}C$. The cold water layer in LowResDoubleMelt thinned more than in the LowResControl. For Disko Bay, both deep troughs (UT and DBT) hold warmer water in LowResDoubleMelt ($3\,^{\circ}C$, Fig. 11d) than in LowResControl ($\sim 2\,^{\circ}C$, Fig. 11c). The maximum increase occurred in a warm core in both troughs, UT and DBT (at kilometre marker 150 km and 400 km), with a depth of 150 m to 350 m. The cooler water layer at the surface again thinned in LowResDoubleMelt (Fig. 11c). However, when examining average velocities normal to the section, for the entire period there was no clear trend that increasing the meltwater strengthens the velocities.

Previous studies, from a variety of scales of modelling, have shown that additional freshwater can increase the presence of heat to a region. In the ocean, if GrIS melt increases, it may add more energetic plume dynamics along a glacier face and increase the strength of the thermohaline circulation in fjords. Cai et al. (2017) showed in a 2–D model, ran for one year, with ice shelf melt derived from observed melt rates for Petermann Glacier, that an increase in thermohaline circulation in the fjord can bring more heat and salt towards the ice sheet. Castro de la Guardia et al. (2015) used a regional ocean model to set up eight sensitivity experiments, adjusting melt rates from the GrIS and ran for a period of 10 years. Grivault et al. (2017) also used a regional ocean model, and had interannual runoff and had experiments run for a 40 year period. With an increase in the GrIS melt, the heat content increases in Baffin Bay (Castro de la Guardia et al., 2015; Grivault et al., 2017).

Of all the regions around Greenland, Baffin Bay is a unique system, as it responds to an increase in the GrIS melt in a different way than the two other regions around Greenland considered in this study. Identifying that ocean temperatures in troughs in Baffin Bay are indeed warming with increasing the GrIS melt provides further support to the work by Castro de la Guardia et al. (2015). This study, however, provides more realistic experiments and analysis on specific locations concerning troughs which connect to fjords with large marine terminating glaciers. Therefore, with an increase in GrIS melt, Baffin Bay's

ocean heat content may increase. Thus increasing the potential for glaciers to continue to melt, impacting climate, SLR, and ecosystems.

3.4 Impact of high frequency atmospheric events

A question of how the atmospheric variability may impact the region of HG for renewing heat from the shelf has been discussed in previous observational studies (Straneo et al., 2010; Christoffersen et al., 2011). How does filtering out storms, where winds and the associated temperatures are impacted, affect the high variability in the south-east? A comparison of LowResControl and LowResNoStorms will be shown.

Figure 12a shows the EKE integrated over the entire depth for the south-east region using LowResControl and Fig. 12b LowResNoStorms. A comparison was done for the north-west and north-east regions, however the south-east region has the highest EKE as well as stronger sensitivity with changes in atmospheric conditions than all other regions. LowResControl (Fig. 12a) had EKE values reaching 4×10^{-3} m^2 s^{-2}. However, LowResNoStorms EKE peaks in magnitudes of 2.5×10^{-3} m^2 s^{-2}, i.e. turbulent energy is reduced by about half. It is clear that the EKE decreases closer to HGT2 where the bathymetry reaches depths of 500 m in the LowResControl (Fig. 12a). It appears that filtering out storms, decreases the EKE strength in the south-east region (Fig. 12b).

Figure 12c and Fig. 12d show the trend of mean heat flux and fluctuation of the heat flux on or off shelf component for HGT2 with the LowResNoStorms. The mean heat flux appears to be smaller in LowResNoStorms than LowResControl. The LowResNoStorms mean component of the onshore heat flux reached values closer to 10 TW in 2004 to end of 2007. LowResControl had onshore heat flux values greater than 5 TW in 2004, 2010, 2015 and 2016. The fluctuation component of the heat flux is smaller with the LowResNoStorms. Therefore storms decreases the fluctuation component of the heat flux and increases the mean component of the heat flux. There is less mean winds from the north towards south and therefore less upper water Ekman transport towards the shelf and fjords. With less Ekman transport of deeper waters away from the fjords, the warm waters present within the deeper layers, therefore they can stay more easily within the fjord. As a result, less storms may increase the overall onshore heat flux into HGT2, as the changes in mean values exceed the changes fluctuation values (~ 5 TW vs ~ 1 TW).

The summation of the onshore heat flux from 2004 to 2016 has been calculated and compared between LowResControl and LowResNoStorms. LowResNoStorms has a total of 2260.2 TW, and the LowResControl is ~ 18 % less, with a total of 1914.5 TW. This extra 345.7 TW could have the potential to melt 1037.1 kilotons of ice per second. Therefore this increase in total onshore heat flux might be due to less heat being transferred off the shelf due to high variability atmospheric forcing.

4 Conclusions

The oceanic heat available in Greenland's troughs is dependent on both the location of the trough, variability of the warm water origin, how the water is transformed as it travels to the troughs, as well as local processes occurring, such as heat loss to the atmosphere. It is important to understand the processes that bring this warm water to the shelf and into the troughs, as this

water can be then exchanged into the fjords. Warm water ~~that exists~~ in fjords ~~creates an~~ oceanic heat forcing on the marine terminating glaciers (Rignot et al., 2016b; Cai et al., 2017; Wood et al., 2018). To our knowledge this is the first ~~look~~ at changes in heat flux in troughs that are connected to fjords with marine terminating glaciers.

This study showed that the presence of warm water at depth can extend far north into Baffin Bay, reaching as north as Melville Bay and its subsequent troughs. The study's model experiments showed that Melville Bay troughs experienced an increased heat flux. Therefore an increase in ocean heat presence in these troughs may have driven more heat to glaciers that terminate here. In 2004 to 2006, model experiments captured an increase in onshore heat flux in DBT, coinciding with the timing of the disintegration of JI floating tounge and within the period of observed oceanic heat increase Disko Bay (from 1997 to 2007) (Holland et al., 2008).

Seasonality of the maximum onshore heat flux through troughs around the GrIS differs due to distance away from the the Irminger Sea. The seasonality of the maximum onshore heat flux through all six regions were presented. For the Irminger Current influence the peaks begin: June for HGT2, July for DBT and September for MVBCT. Then for the areas receiving warm water from the NwAC: August for KT, November for SBS, and September to January for NT.

The south-east region has the highest EKE as well as stronger sensitivity with changes in atmospheric conditions than all other regions. The south-east coast of Greenland is impacted the most by the atmospheric filter (i.e. no storms). No storms resulted in a reduction of EKE (~ 50 %) and less offshore heat transport and therefore more heat flux (~ 20 %) through the Helheim glacier trough (HGT2).

It is imperative to try to understand how sensitive the ocean is to additional meltwater from Greenland. Baffin Bay is a unique system, as it responds to an increase in the GrIS melt in a different way than any other region around Greenland. Baffin Bay troughs will bring more heat (~ 40 %) towards the GrIS if the GrIS freshwater flux doubles. This study shows that a doubling of the GrIS melt may cause a warming in Baffin Bay and an increase in heat flux through troughs, potentially escalating the melt of the GrIS, consistent with Castro de la Guardia et al. (2015) but now in a more realistic set–up with Greenland meltwater temporally and spatially distributed.

Since the model used in this study does not have the capability to resolve small scale processes such as fjord circulation, the exchange between fjords and troughs cannot be looked into. Instead, there is an assumption in place, that the water characteristics that exist in the troughs will match those in the fjords due to dynamics of cross shelf exchanges (Jackson et al., 2014; Sutherland et al., 2014). A warming of ocean ~~heat~~ in troughs may lead to a warming of ocean heat to fjords. Due to the model bathymetry under representing the depth of these troughs, this study may be underestimating the amount of ocean heat available to enter these troughs. The study only looked at the impact from the freshwater flux of the GrIS. The inclusion of an iceberg model coupled with an ocean model may give further insight to the heat and freshwater budget in regions of high GrIS discharge, such as explained in Marson et al. (2018).

Author contributions. L.G. and P.M. designed the study and L.G. carried it out. X.H. developed the model configuration and performed the simulations. L.G. prepared the manuscript with contributions from all co-authors. M.R. and C.L. provided comments on the manuscript, with C.L. also provided Davis Strait transport data.

Competing interests. No competing interest are present.

5 *Disclaimer.* TEXT

Acknowledgements. We would like to thank Yarisbel Garcia Quintana for carrying out the LowResNoStorm experiment. We are grateful to the NEMO development team and the Drakkar project for providing the model and continuous guidance, and to Westgrid and Compute Canada for computational resources, where all model experiments were performed and archived (http://www.computecanada.ca). We gratefully acknowledge the financial and logistic support of grants from the Natural Sciences and Engineering Research Council (NSERC) of
10 Canada. These include Discovery Grant (rgpin227438) awarded to Dr. P.G. Myers, Climate Change and Atmospheric Research Grant (VITALS - RGPCC 433898), and an International Create (ArcTrain - 432295). The author would like to thank the anonymous reviewers for their insightful comments and suggestions that have contributed to improving this paper.

References

Aagaard, K. and Carmack, E. C.: The role of sea ice and other fresh water in the Arctic circulation, Journal of Geophysical Research: Oceans, 94, 14 485–14 498, https://doi.org/10.1029/JC094iC10p14485, 1989.

Aksenov, Y., Bacon, S., Coward, A. C., and Holliday, N. P.: Polar outflow from the Arctic Ocean: A high resolution model study, Journal of Marine Systems, 83, 14 – 37, https://doi.org/http://dx.doi.org/10.1016/j.jmarsys.2010.06.007, 2010.

Amante, C. and Eakins, B.: ETOPO1 1 Arc-Minute Global Relief Model: Procedures, Data Sources and Analysis, NOAA Technical Memorandum NESDIS NGDC-24, https://doi.org/10.7289/V5C8276M, 2009.

An, L., Rignot, E., Elieff, S., Morlighem, M., Millan, R., Mouginot, J., Holland, D. M., Holland, D., and Paden, J.: Bed elevation of Jakobshavn Isbrae, West Greenland, from high-resolution airborne gravity and other data, Geophysical Research Letters, 44, 3728–3736, https://doi.org/10.1002/2017GL073245, http://dx.doi.org/10.1002/2017GL073245, 2017GL073245, 2017.

Arrigo, K. R., van Dijken, G. L., Castelao, R. M., Luo, H., Rennermalm, s. K., Tedesco, M., Mote, T. L., Oliver, H., and Yager, P. L.: Melting glaciers stimulate large summer phytoplankton blooms in southwest Greenland waters, Geophysical Research Letters, 44, 6278–6285, https://doi.org/10.1002/2017GL073583, https://agupubs.onlinelibrary.wiley.com/doi/abs/10.1002/2017GL073583, 2017.

Azetsu-Scott, K. and Tan, F. C.: Oxygen isotope studies from Iceland to an East Greenland Fjord: behaviour of glacial meltwater plume, Marine Chemistry, 56, 239 – 251, https://doi.org/http://dx.doi.org/10.1016/S0304-4203(96)00078-3, http://www.sciencedirect.com/science/article/pii/S0304420396000783, modern Chemical and Biological Oceanography: The Influence of Peter J. Wangersky, 1997.

Bacon, S., Marshall, A., Holliday, N. P., Aksenov, Y., and Dye, S. R.: Seasonal variability of the East Greenland Coastal Current, Journal of Geophysical Research: Oceans, 119, 3967–3987, https://doi.org/10.1002/2013JC009279, 2014.

Bamber, J., Van Den Broeke, M., Ettema, J., Lenaerts, J., and Rignot, E.: Recent large increases in freshwater fluxes from Greenland into the North Atlantic, Geophysical Research Letters, 39, 2012.

Bamber, J. L., Griggs, J. A., Hurkmans, R. T. W. L., Dowdeswell, J. A., Gogineni, S. P., Howat, I., Mouginot, J., Paden, J., Palmer, S., Rignot, E., and Steinhage, D.: A new bed elevation dataset for Greenland, The Cryosphere, 7, 499–510, https://doi.org/10.5194/tc-7-499-2013, 2013.

Barnier, B., Brodeau, L., Le Sommer, J., Molines, J., Penduff, T., Theetten, S., Treguier, A. M., Madec, G., Biastoch, A., Bőning, C., Dengg, J., Gulev, S., Bourdallé, B. R., Chanut, J., Garric, G., Alderson, S., Coward, A., de Cuevas, B., New, A., Haines, K., Smith, G., Drijfhout, S., Hazeleger, W., Severijns, C., and Myers, P.: Eddy-permitting ocean circulation hindcasts of past decades, CLIVAR Exchanges, 12, 8–10, 2007.

Bartholomaus, T. C., Stearns, L. A., Sutherland, D. A., Shroyer, E. L., Nash, J. D., Walker, R. T., Catania, G., Felikson, D., Carroll, D., Fried, M. J., and et al.: Contrasts in the response of adjacent fjords and glaciers to ice-sheet surface melt in West Greenland, Annals of Glaciology, 57, 25–38, https://doi.org/10.1017/aog.2016.19, 2016.

Beaird, N., Straneo, F., and Jenkins, W.: Characteristics of meltwater export from Jakobshavn Isbræ and Ilulissat Icefjord, Annals of Glaciology, 58, 107–117, https://doi.org/10.1017/aog.2017.19, 2017.

Beaird, N. L., Straneo, F., and Jenkins, W.: Export of Strongly Diluted Greenland Meltwater From a Major Glacial Fjord, Geophysical Research Letters, 45, 4163–4170, https://doi.org/10.1029/2018GL077000, https://agupubs.onlinelibrary.wiley.com/doi/abs/10.1029/2018GL077000, 2018.

Bernard, B., Madec, G., Penduff, T., Molines, J.-M., Treguier, A.-M., Le Sommer, J., Beckmann, A., Biastoch, A., Böning, C., Dengg, J., Derval, C., Durand, E., Gulev, S., Remy, E., Talandier, C., Theetten, S., Maltrud, M., McClean, J., and De Cuevas, B.: Impact of partial

steps and momentum advection schemes in a global ocean circulation model at eddy-permitting resolution, Ocean Dynamics, 56, 543–567, https://doi.org/10.1007/s10236-006-0082-1, https://doi.org/10.1007/s10236-006-0082-1, 2006.

Beszczynska-Möller, A., Fahrbach, E., Schauer, U., and Hansen, E.: Variability in Atlantic water temperature and transport at the entrance to the Arctic Ocean, 1997–2010, ICES Journal of Marine Science: Journal du Conseil, https://doi.org/10.1093/icesjms/fss056, 2012.

5 BODC: British Oceanographic Data Center's General Bathymetric Chart of the Oceans, 2008.

Boning, C. W., Behrens, E., Biastoch, A., Getzlaff, K., and Bamber, J. L.: Emerging impact of Greenland meltwater on deepwater formation in the North Atlantic Ocean, Nature Geosci, 9, 523–527, https://doi.org/10.1038/ngeo2740, 2016.

Box, J. E.and Yang, L., Bromwich, D. H., and Bai, L.: Greenland Ice Sheet Surface Air Temperature Variability: 1840–2007, Journal of Climate, 22, 4029–4049, https://doi.org/10.1175/2009JCLI2816.1, 2009.

10 Cai, C., Rignot, E., Menemenlis, D., and Nakayama, Y.: Observations and modeling of ocean-induced melt beneath Petermann Glacier Ice Shelf in northwestern Greenland, Geophysical Research Letters, https://doi.org/10.1002/2017GL073711, http://dx.doi.org/10.1002/2017GL073711, 2017.

Carroll, D., Sutherland, D. A., Curry, B., Nash, J. D., Shroyer, E. L., Catania, G. A., Stearns, L. A., Grist, J. P., Lee, C. M., and de Steur, L.: Subannual and Seasonal Variability of Atlantic-Origin Waters in Two Adjacent West Greenland Fjords, Journal of Geo-
15 physical Research: Oceans, 123, 6670–6687, https://doi.org/10.1029/2018JC014278, https://agupubs.onlinelibrary.wiley.com/doi/abs/10.1029/2018JC014278, 2018.

Castro de la Guardia, L., Hu, X., and Myers, P. G.: Potential positive feedback between Greenland Ice Sheet melt and Baffin Bay heat content on the west Greenland shelf, Geophysical Research Letters, 42, 4922–4930, https://doi.org/10.1002/2015GL064626, 2015.

Christoffersen, P., Mugford, R. I., Heywood, K. J., Joughin, I., Dowdeswell, J. A., Syvitski, J. P. M., Luckman, A., and Benham, T. J.:
20 Warming of waters in an East Greenland fjord prior to glacier retreat: Mechanisms and connection to large-scale atmospheric conditions, Cryosphere, 5, 701–714, 2011.

Csatho, B. M., Schenk, A. F., van der Veen, C. J., Babonis, G., Duncan, K., Rezvanbehbahani, S., van den Broeke, M. R., Simonsen, S. B., Nagarajan, S., and van Angelen, J. H.: Laser altimetry reveals complex pattern of Greenland Ice Sheet dynamics, Proceedings of the National Academy of Sciences, 111, 18 478–18 483, https://doi.org/10.1073/pnas.1411680112, http://www.pnas.org/content/111/52/
25 18478, 2014.

Curry, B., Lee, C. M., and Petrie, B.: Volume, Freshwater, and Heat Fluxes through Davis Strait, 2004–05, Journal of Physical Oceanography, 41, 429–436, https://doi.org/10.1175/2010JPO4536.1, https://doi.org/10.1175/2010JPO4536.1, 2011.

Curry, B., Lee, C., Petrie, B., Moritz, R., and Kwok, R.: Multiyear volume, liquid freshwater, and sea ice transports through Davis Strait, 2004-10, Journal of Physical Oceanography, 44, 1244–1266, https://doi.org/10.1175/JPO-D-13-0177.1, 2014.

30 Dai, A., Qian, T., Trenberth, K. E., and Milliman, J. D.: Changes in continental freshwater discharge from 1948 to 2004, Journal of Climate, 22, 2773–2792, 2009.

Dukhovskoy, D. S., Myers, P. G., Platov, G., Timmermans, M.-L., Curry, B., Proshutinsky, A., Bamber, J. L., Chassignet, E., Hu, X., Lee, C. M., and Somavilla, R.: Greenland freshwater pathways in the sub-Arctic Seas from model experiments with passive tracers, Journal of Geophysical Research: Oceans, https://doi.org/10.1002/2015JC011290, 2016.

35 Eskridge, R. E., Ku, J. Y., Rao, S. T., Porter, P. S., and Zurbenko, I. G.: Separating Different Scales of Motion in Time Series of Meteorological Variables, Bulletin of the American Meteorological Society, 78, 1473–1484, https://doi.org/10.1175/1520-0477(1997)078<1473:SDSOMI>2.0.CO;2, https://doi.org/10.1175/1520-0477(1997)078<1473:SDSOMI>2.0.CO;2, 1997.

Felikson, D., Bartholomaus, T. C., Catania, G. A., Korsgaard, N. J., Kjær, K. H., Morlighem, M., Noël, B., van den Broeke, M., Stearns, L. A., Shroyer, E. L., Sutherland, D. A., and Nash, J. D.: Inland thinning on the Greenland Ice Sheet controlled by outlet glacier geometry, Nature Geoscience, 10, 366–369, https://doi.org/10.1038/ngeo2934, 2017.

Fenty, I., Willis, J. K., Khazendar, A., Dinardo, S., Forsberg, R., Fukumori, I., Holland, D., Jakobsson, M., Moller, D., Münchow, J. M. A., Rignot, E., Schodlok, M., Thompson, A. F., Tinto, K., Rutherford, M., and Trenholm, N.: Oceans Melting Greenland: Early Results from NASA's Ocean-Ice Mission in Greenland , Oceanography, 29, https://doi.org/10.5670/oceanog.2016.100, 2016.

Ferry, N., Greiner, E., Garric, G., Penduff, T., Treiguier, A.-M., and Reverdin, G.: GLORYS-1 Reference Manual for Stream 1 (2002-2007), GLORYS project report, 2008.

Fichefet, T. and Morales Maqueda, M.: Sensitivity of a global sea ice model to the treatment of ice thermodynamics and dynamics, Journal of Geophysical Research, 102, 12 609–12 646, 1997.

Fratantoni, P. S. and Pickart, R. S.: The western North Atlantic shelfbreak current system in summer, Journal of Physical Oceanography, 37, 2509–2533, 2007.

Garcia-Quintana, Y., Courtois, P., Hu, X., Pennelly, C., Kieke, D., and Myers, P. G.: Sensitivity of Labrador Sea Water formation to changes in model resolution, atmospheric forcing and freshwater input, Journal of Geophysical Research: Oceans, 0, 2019.

Gillard, L. C., Hu, X., Myers, P. G., and Bamber, J. L.: Meltwater pathways from marine terminating glaciers of the Greenland Ice Sheet, Geophysical Research Letters, 43, 10,873–10,882, https://doi.org/10.1002/2016GL070969, http://dx.doi.org/10.1002/2016GL070969, 2016.

Gladish, C., Holland, D., and Lee, C.: Oceanic boundary conditions for Jakobshavn Glacier. Part II: Provenance and sources of variability of disko bay and Ilulissat Icefjord waters, 1990-2011, Journal of Physical Oceanography, 45, 33–63, https://doi.org/10.1175/JPO-D-14-0045.1, 2015a.

Gladish, C., Holland, D., Rosing-Asvid, A., Behrens, J., and Boje, J.: Oceanic boundary conditions for Jakobshavn Glacier. Part I: Variability and renewal of Ilulissat Icefjord waters, 2001-14, Journal of Physical Oceanography, 45, 3–32, https://doi.org/10.1175/JPO-D-14-0044.1, 2015b.

Grivault, N., Hu, X., and Myers, P. G.: Evolution of Baffin Bay Water Masses and Transports in a Numerical Sensitivity Experiment under Enhanced Greenland Melt, Atmosphere-Ocean, 55, 169–194, https://doi.org/10.1080/07055900.2017.1333950, http://dx.doi.org/10.1080/07055900.2017.1333950, 2017.

Hogan, K. A., Cofaigh, C. ., Jennings, A. E., Dowdeswell, J. A., and Hiemstra, J. F.: Deglaciation of a major palaeo-ice stream in Disko Trough, West Greenland, Quaternary Science Reviews, 147, 5 – 26, https://doi.org/https://doi.org/10.1016/j.quascirev.2016.01.018, http://www.sciencedirect.com/science/article/pii/S0277379116300208, special Issue: PAST Gateways (Palaeo-Arctic Spatial and Temporal Gateways), 2016.

Holdsworth, A. M. and Myers, P. G.: The Influence of High-Frequency Atmospheric Forcing on the Circulation and Deep Convection of the Labrador Sea, Journal of Climate, 28, 4980–4996, https://doi.org/10.1175/JCLI-D-14-00564.1, https://doi.org/10.1175/JCLI-D-14-00564.1, 2015.

Holland, D. M., Thomas, R. H., De Young, B., Ribergaard, M. H., and Lyberth, B.: Acceleration of Jakobshavn Isbrae triggered by warm subsurface ocean waters, Nature Geoscience, 1, 659–664, 2008.

Hu, X. and Myers, P. G.: A Lagrangian view of Pacific water inflow pathways in the Arctic Ocean during model spin-up, Ocean Modelling, 71, 66 – 80, https://doi.org/http://dx.doi.org/10.1016/j.ocemod.2013.06.007, 2013.

Inall, M. E., Murray, T., Cottier, F. R., Scharrer, K., Boyd, T. J., Heywood, K. J., and Bevan, S. L.: Oceanic heat delivery via Kangerdlugssuaq Fjord to the south-east Greenland Ice Sheet, Journal of Geophysical Research: Oceans, 119, 631–645, https://doi.org/10.1002/2013JC009295, 2014.

Jackson, R. H., Straneo, F., and Sutherland, D. A.: Externally forced fluctuations in ocean temperature at Greenland glaciers in non-summer
5   months, Nature Geoscience, 7, 503–508, 2014.

Jenkins, A.: Convection-driven melting near the grounding lines of ice shelves and tidewater glaciers, Journal of Physical Oceanography, 41, 2279–2294, 2011.

Joughin, I., Alley, R. B., and Holland, D. M.: Ice-Sheet Response to Oceanic Forcing, Science, 338, 1172–1176, https://doi.org/10.1126/science.1226481, 2012.

10   Karcher, M., Beszczynska-Möller, A., Kauker, F., Gerdes, R., Heyen, S., Rudels, B., and Schauer, U.: Arctic Ocean warming and its consequences for the Denmark Strait overflow, Journal of Geophysical Research: Oceans, 116, https://doi.org/10.1029/2010JC006265, 2011.

Khazendar, A., Fenty, I. G., Carroll, D., Gardner, A. an Lee, C. M., Fukumori, I., Wang, O., Zhang, H., Seroussi, H., Moller, D., Noël, B. P. Y., van den Broeke, M. R., Dinardo, S., and Willis, J.: Interruption of two decades of Jakobshavn Isbrae acceleration and thinning as regional ocean cools, Nature Geoscience, 12, https://doi.org/10.1038/s41561-019-0329-3, https://doi.org/10.1038/s41561-019-0329-3, 2019.

15   Luo, H., Castelao, R. M., Rennermalm, A. K., Tedesco, M., Bracco, A., Yager, P. L., and Mote, T. L.: Oceanic transport of surface meltwater from the southern Greenland Ice Sheet, Nature Geoscience, https://doi.org/10.1038/ngeo2708, 2016.

Madec, G.: NEMO ocean engine, Note du Pole de modélisation, 2008.

Marson, J. M., Myers, P. G., Hu, X., and Le Sommer, J.: Using Vertically Integrated Ocean Fields to Characterize Greenland Icebergs' Distribution and Lifetime, Geophysical Research Letters, 45, 4208–4217, https://doi.org/10.1029/2018GL077676, https://agupubs.onlinelibrary.
20   wiley.com/doi/abs/10.1029/2018GL077676, 2018.

Mayer, C., Reeh, N., Jung-Rothenhäusler, F., Huybrechts, P., and Oerter, H.: The subglacial cavity and implied dynamics under Nioghalvfjerdsfjorden Glacier, NE-Greenland, Geophysical Research Letters, 27, 2289–2292, https://doi.org/10.1029/2000GL011514, https://agupubs.onlinelibrary.wiley.com/doi/abs/10.1029/2000GL011514, 2000.

MEOM: Bathymetry ORCA0.25, http://servdap.legi.grenoble-inp.fr/meom/ORCA025-I/, 2013.

25   Moon, T., Joughin, I., and Smith, B.: Seasonal to multiyear variability of glacier surface velocity, terminus position, and sea ice/ice mélange in northwest Greenland, Journal of Geophysical Research: Earth Surface, 120, 818–833, https://doi.org/10.1002/2015JF003494, https://agupubs.onlinelibrary.wiley.com/doi/abs/10.1002/2015JF003494, 2015.

Morlighem, M., Williams, C. N., Rignot, E., An, L., Arndt, J. E., Bamber, J. L., Catania, G., Chauché, N., Dowdeswell, J. A., Dorschel, B., Fenty, I., Hogan, K., Howat, I., Hubbard, A., Jakobsson, M., Jordan, T. M., Kjeldsen, K. K., Millan, R., Mayer, L., Mouginot, J.,
30   Noël, B. P. Y., O'Cofaigh, C., Palmer, S., Rysgaard, S., Seroussi, H., Siegert, M. J., Slabon, P., Straneo, F., van den Broeke, M. R., Weinrebe, W., Wood, M., and Zinglersen, K. B.: BedMachine v3: Complete Bed Topography and Ocean Bathymetry Mapping of Greenland From Multibeam Echo Sounding Combined With Mass Conservation, Geophysical Research Letters, 44, 11,051–11,061, https://doi.org/10.1002/2017GL074954, https://agupubs.onlinelibrary.wiley.com/doi/abs/10.1002/2017GL074954, 2017.

Myers, P. G. and Ribergaard, M. H.: Warming of the polar water layer in Disko Bay and potential impact on Jakobshavn Isbrae, Journal of
35   Physical Oceanography, 43, 2629–2640, 2013.

Myers, P. G., Donnelly, C., and Ribergaard, M. H.: Structure and variability of the West Greenland Current in Summer derived from 6 repeat standard sections, Progress in Oceanography, 80, 93–112, 2009.

Porter, D. F., Tinto, K. J., Boghosian, A., Cochran, J. R., Bell, R. E., Manizade, S. S., and Sonntag, J. G.: Bathymetric control of tidewater glacier mass loss in northwest Greenland, Earth and Planetary Science Letters, 401, 40 – 46, https://doi.org/https://doi.org/10.1016/j.epsl.2014.05.058, http://www.sciencedirect.com/science/article/pii/S0012821X14003744, 2014.

Rastner, P., Bolch, T., Mölg, N., Machguth, H., Le Bris, R., and Paul, F.: The first complete inventory of the local glaciers and ice caps on Greenland, The Cryosphere, 6, 1483–1495, https://doi.org/10.5194/tc-6-1483-2012, https://www.the-cryosphere.net/6/1483/2012/, 2012.

Ribergaard, M. H.: Oceanographic Investigations off West Greenland 2013, NAFO Scientific Council Documents, 14/001, 2014.

Rignot, E. and Kanagaratnam, P.: Changes in the velocity structure of the Greenland Ice Sheet, Science, 311, 986–990, 2006.

Rignot, E. and Mouginot, J.: Ice flow in Greenland for the International Polar Year 2008-2009, Geophysical Research Letters, 39, 2012.

Rignot, E., Fenty, I., Xu, Y., Cai, C., Velicogna, I., Cofaigh, C. ., Dowdeswell, J. A., Weinrebe, W., Catania, G., and Duncan, D.: Bathymetry data reveal glaciers vulnerable to ice-ocean interaction in Uummannaq and Vaigat glacial fjords, west Greenland, Geophysical Research Letters, 43, 2667–2674, https://doi.org/10.1002/2016GL067832, http://dx.doi.org/10.1002/2016GL067832, 2016GL067832, 2016a.

Rignot, E., Xu, Y., Menemenlis, D., Mouginot, J., Scheuchl, B., Li, X., Morlighem, M., Seroussi, H., den Broeke, M. v., Fenty, I., Cai, C., An, L., and Fleurian, B. d.: Modeling of ocean-induced ice melt rates of five west Greenland glaciers over the past two decades, Geophysical Research Letters, 43, 6374–6382, https://doi.org/10.1002/2016GL068784, https://agupubs.onlinelibrary.wiley.com/doi/abs/10.1002/2016GL068784, 2016b.

Schaffer, J., von Appen, W.-J., Dodd, P. A., Hofstede, C., Mayer, C., de Steur, L., and Kanzow, T.: Warm water pathways toward Nioghalvfjerdsfjorden Glacier, Northeast Greenland, Journal of Geophysical Research: Oceans, 122, 4004–4020, https://doi.org/10.1002/2016JC012462, https://agupubs.onlinelibrary.wiley.com/doi/abs/10.1002/2016JC012462, 2017.

Seroussi, H., Morlighem, M., Rignot, E., Larour, E., Aubry, D., Ben Dhia, H., and Kristensen, S. S.: Ice flux divergence anomalies on 79north Glacier, Greenland, Geophysical Research Letters, 38, https://doi.org/10.1029/2011GL047338, http://dx.doi.org/10.1029/2011GL047338, l09501, 2011.

Slabon, P., Dorschel, B., Jokat, W., Myklebust, R., Hebbeln, D., and Gebhardt, C.: Greenland ice sheet retreat history in the northeast Baffin Bay based on high-resolution bathymetry, Quaternary Science Reviews, 154, 182 – 198, https://doi.org/http://dx.doi.org/10.1016/j.quascirev.2016.10.022, http://www.sciencedirect.com/science/article/pii/S0277379116304930, 2016.

Smith, G. C., Roy, F., Mann, P., Dupont, F., Brasnett, B., Lemieux, J.-F., Laroche, S., and Bélair, S.: A new atmospheric dataset for forcing ice-ocean models: Evaluation of reforecasts using the Canadian global deterministic prediction system, Quarterly Journal of the Royal Meteorological Society, 140, 881–894, 2014.

Smith, W. H. F. and Sandwell, D. T.: Global seafloor topography from satellite altimetry and ship depth soundings, Science, 277, 1957–1962, 1997.

Straneo, F.: Heat and freshwater transport through the central Labrador Sea, Journal of Physical Oceanography, 36, 606–628, 2006.

Straneo, F. and Heimbach, P.: North Atlantic warming and the retreat of Greenland's outlet glaciers, Nature, 504, 36–43, 2013.

Straneo, F., Hamilton, G., Sutherland, D., Stearns, L. A., Davidson, F., Hammill, M., Stenson, G. B., and A., R.: Rapid circulation of warm subtropical waters in a major glacial fjord in East Greenland, Nature Geosci, 3, 182–186),, 2010.

Straneo, F., Sutherland, D. A., Holland, D., Gladish, C., Hamilton, G. S., Johnson, H. L., Rignot, E., Xu, Y., and Koppes, M.: Characteristics of ocean waters reaching Greenland's glaciers, Annals of Glaciology, 53, 202–210, 2012.

Sutherland, D. A., Straneo, F., and Pickart, R. S.: Characteristics and dynamics of two major Greenland glacial fjords, Journal of Geophysical Research: Oceans, 119, 3767–3791, 2014.

Swingedouw, D., Rodehacke, C. B., Olsen, S. M., Menary, M., Gao, Y., Mikolajewicz, U., and Mignot, J.: On the reduced sensitivity of the Atlantic overturning to Greenland Ice Sheet melting in projections: a multi-model assessment, Climate Dynamics, 2014.

van den Broeke, M. R., Enderlin, E. M., Howat, I. M., Kuipers Munneke, P., Noël, B. P. Y., van de Berg, W. J., van Meijgaard, E., and Wouters, B.: On the recent contribution of the Greenland Ice Sheet to sea level change, The Cryosphere, 10, 1933–1946, https://doi.org/10.5194/tc-10-1933-2016, https://www.the-cryosphere.net/10/1933/2016/, 2016.

Weijer, W., Maltrud, M. E., Hecht, M. W., Dijkstra, H. A., and Kliphuis, M. A.: Response of the Atlantic Ocean circulation to Greenland Ice Sheet melting in a strongly-eddying ocean model, Geophysical Research Letters, 39, 2012.

Williams, C. N., Cornford, S. L., Jordan, T. M., Dowdeswell, J. A., Siegert, M. J., Clark, C. D., Swift, D. A., Sole, A., Fenty, I., and Bamber, J. L.: Generating synthetic fjord bathymetry for coastal Greenland, The Cryosphere, 11, 363–380, https://doi.org/10.5194/tc-11-363-2017, https://www.the-cryosphere.net/11/363/2017/, 2017.

Wilson, N. J. and Straneo, F.: Water exchange between the continental shelf and the cavity beneath Nioghalvfjerdsbrae (79 North Glacier), Geophysical Research Letters, 42, 7648–7654, https://doi.org/10.1002/2015GL064944, 2015.

Wood, M., Rignot, E., Fenty, I., Menemenlis, D., Millan, R., Morlighem, M., Mouginot, J., and Seroussi, H.: Ocean-Induced Melt Triggers Glacier Retreat in Northwest Greenland, Geophysical Research Letters, 45, 8334–8342, https://doi.org/10.1029/2018GL078024, https://agupubs.onlinelibrary.wiley.com/doi/abs/10.1029/2018GL078024, 2018.

Zurbenko, I., Porter, P. S., Gui, R., Rao, S. T., Ku, J. Y., and Eskridge, R. E.: Detecting Discontinuities in Time Series of Upper-Air Data: Development and Demonstration of an Adaptive Filter Technique, Journal of Climate, 9, 3548–3560, https://doi.org/10.1175/1520-0442(1996)009<3548:DDITSO>2.0.CO;2, https://doi.org/10.1175/1520-0442(1996)009<3548:DDITSO>2.0.CO;2, 1996.
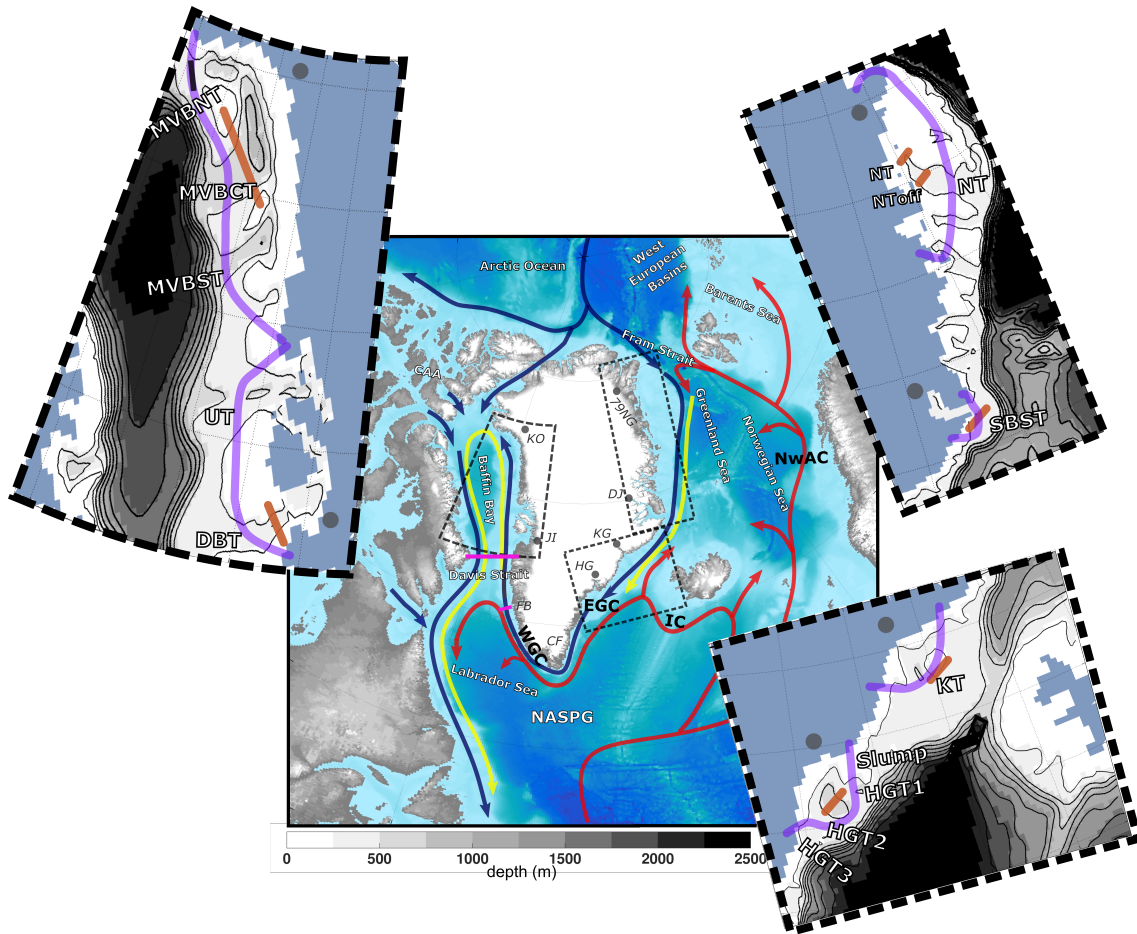
Figure 1. Ocean circulation around Greenland, with relatively warm Atlantic waters are seen in red, modified Atlantic waters in yellow and Arctic and freshwater pathways in blue lines. The large map shows areas that will be discussed throughout this study such as the North Atlantic Subpolar Gyre (NASPG), Labrador Sea, Davis Strait (section drawn in magenta), Baffin Bay, Canadian Arctic Archipelago (CAA), Arctic Ocean, West European Basins, Norwegian Sea, Greenland Sea, Fram Strait, Cape Farwell (CF), and Fylla Bank (FB) (section drawn in magenta) . Ocean currents (adapted from Straneo et al. (2012); Hu and Myers (2013)) that will be discussed are shown here, Irminger Current (IC), Norwegian Atlantic Current (NwAC), East Greenland Current (EGC), and West Greenland Current (WGC). The light grey circles show the locations of six marine terminating glaciers. Kong Oscar (KO) that terminates into Melville Bay (MVB), Jakobshavn Isbrae (JI) that terminates into Disko Bay (DB), Helheim Glacier (HG), Kangerlussuaq Glacier (KG), Daugaard-Jensen Glacier that terminates into Scoresby Sund (SBS) and Nioghalvfjerdsbrae (79NG). The insets show a closer view of this studies specific regions around Greenland. Starting from the top left, the west, south-east, and north-east coast. The insets show the model coastline, model bathymetry in metres (in grey shading and black contours), six sections of our analysis along the shelf in light purple, sections of troughs (tan lines).
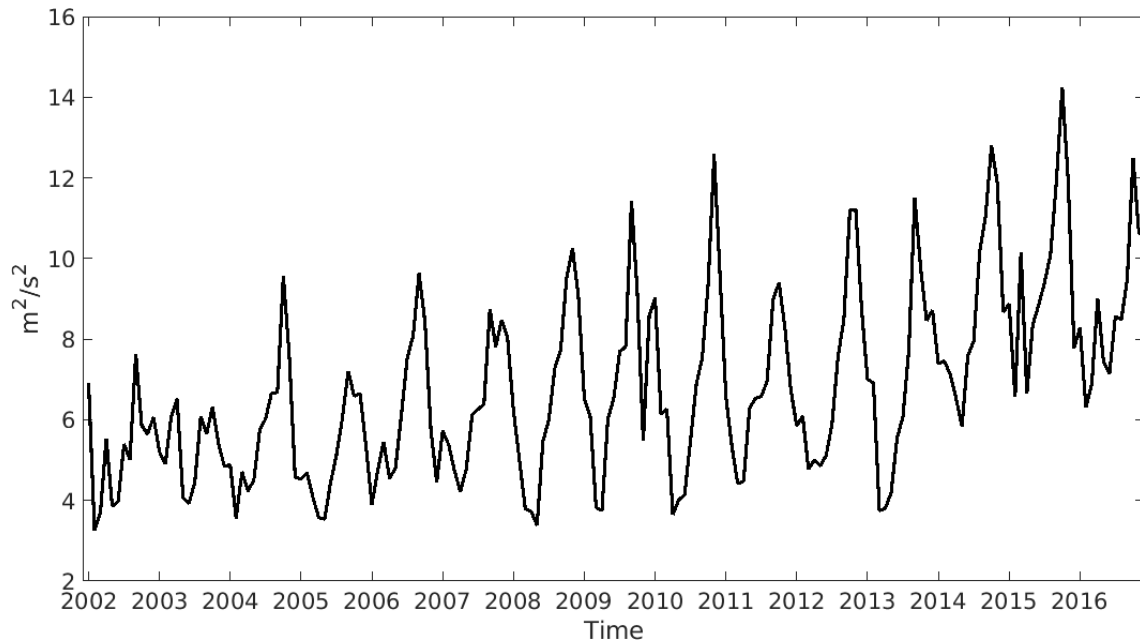
LowResControl (a)
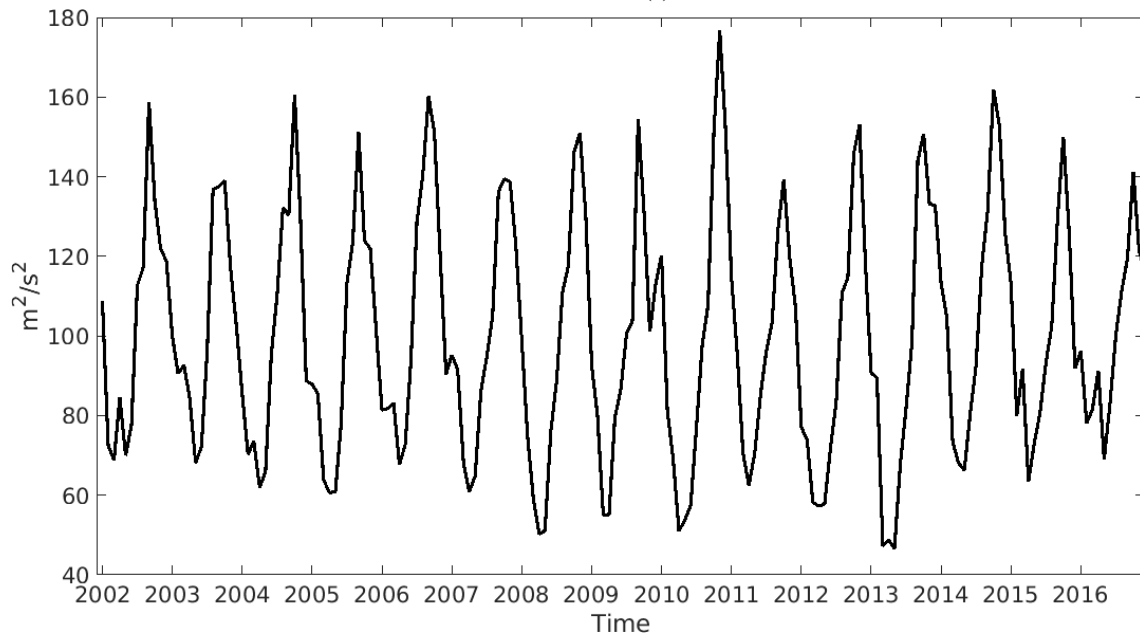
HighRes (b)

Figure 2. Monthly summation of total kinetic energy in Baffin Bay for two configurations, LowResControl and HighRes.
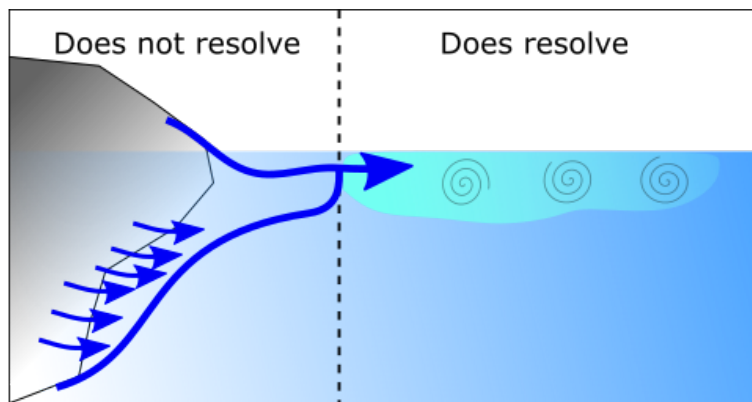
Figure 3. The schematic shows how the model injects meltwater. The left side of the figure shows what the model cannot resolve. This includes a glacier, small scale melting from the glacier, and the plume dynamics that occurs along the face of the glacier. Our model resolves larger scale processes that occur along the coastline, and therefore, injects the meltwater from the GrIS at the first ocean model layer at the surface, and then is mixed to a thickness of 10 m.
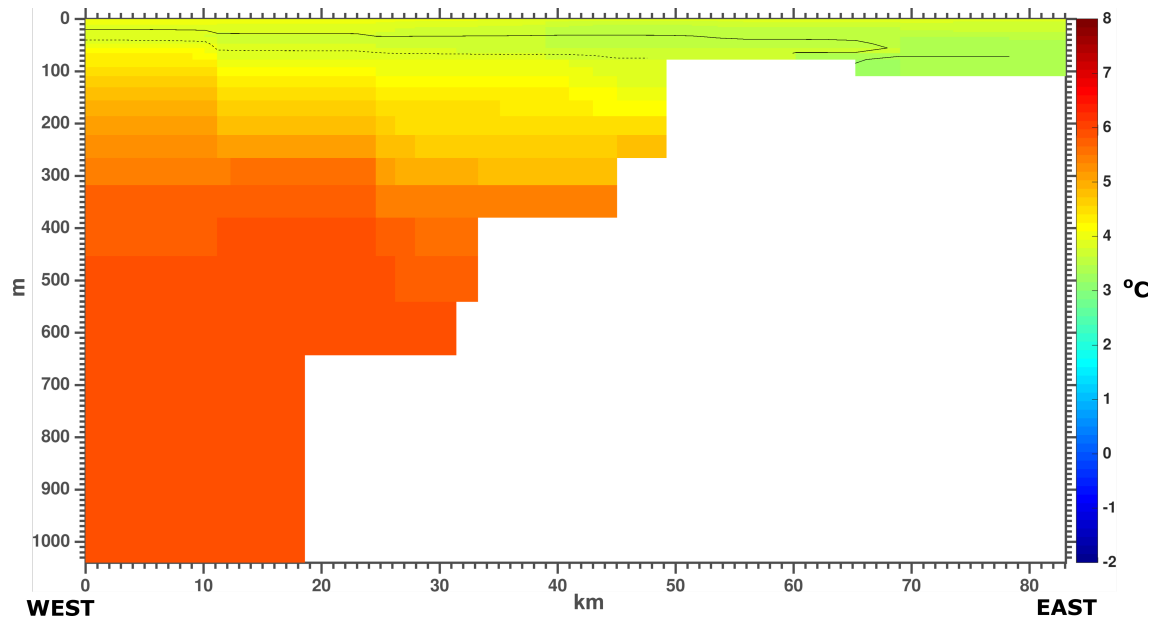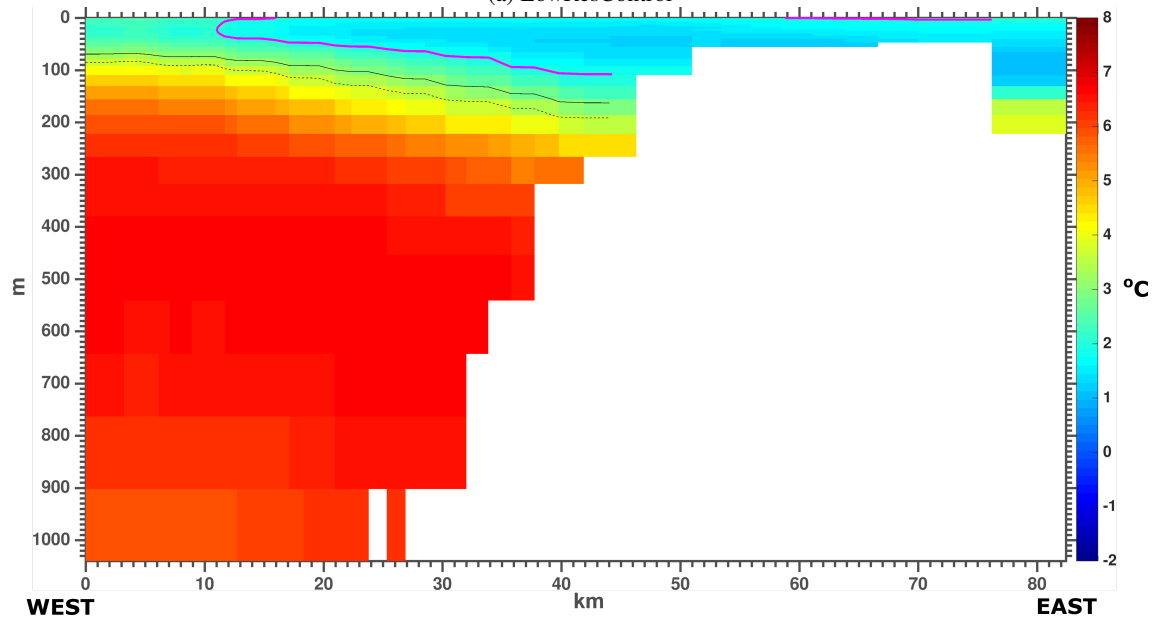
Figure 4. Fylla Bank temperature average for June 2013 for (a) LowResControl and (b) HighRes. Magenta shows temperature of $2\,^{\circ}C$, black line indicates a contour of Salinity of 34, and blacked dashed line indicates a contour of salinity of 34.2.
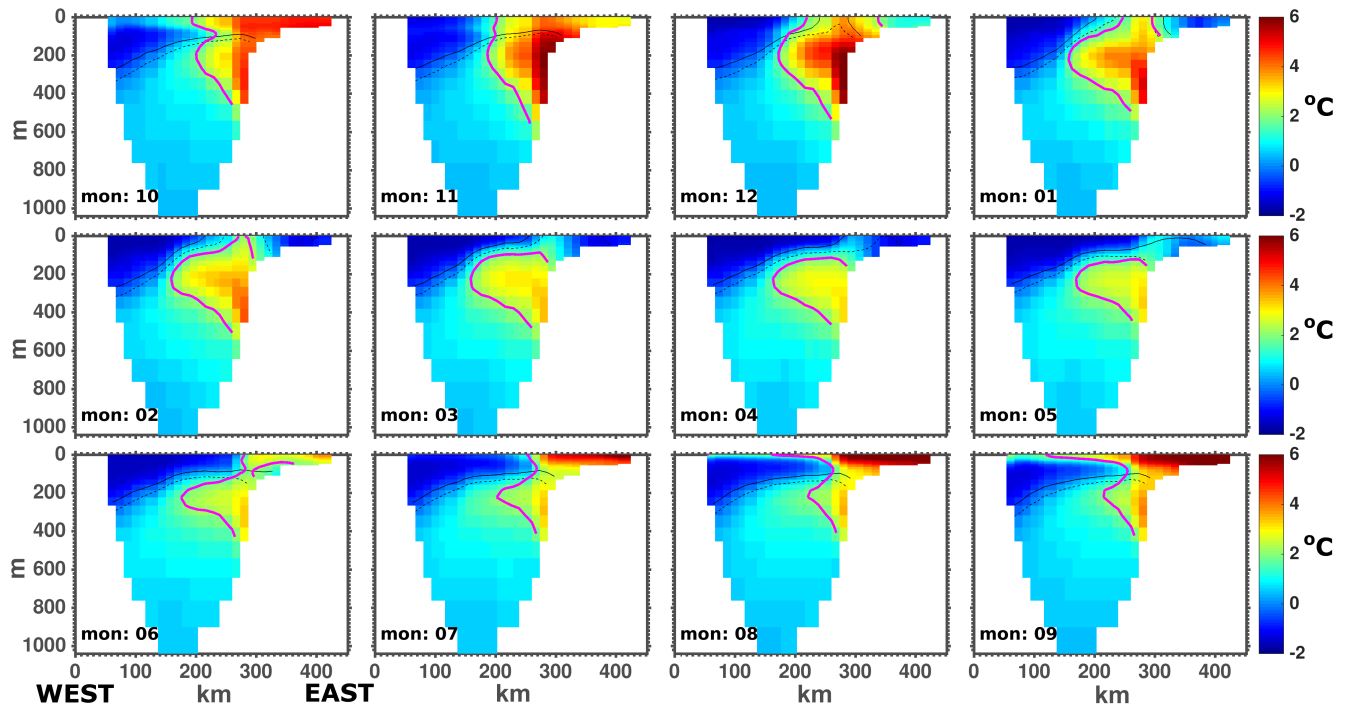
Figure 5. LowResControl average temperature of Davis Strait through the period of 2004 to 2010 at Davis Strait. Magenta shows temperature of $2\,^{\circ}C$, black line indicates a contour of Salinity of 34, and blacked dashed line indicates a contour of salinity of 34.2.
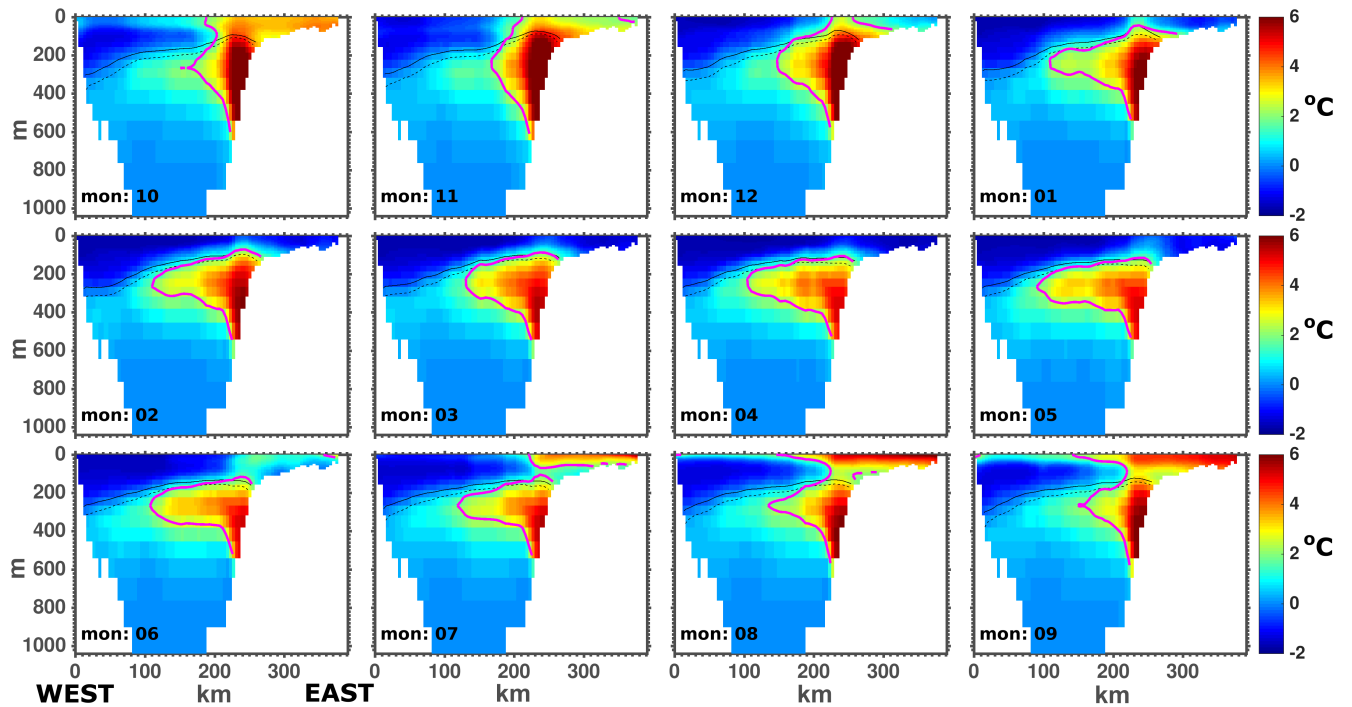
Figure 6. HighRes average temperature of Davis Strait through the period of 2004 to 2010 at Davis Strait. Magenta shows temperature of $2\,^{\circ}C$, black line indicates a contour of Salinity of 34, and blacked dashed line indicates a contour of salinity of 34.2.
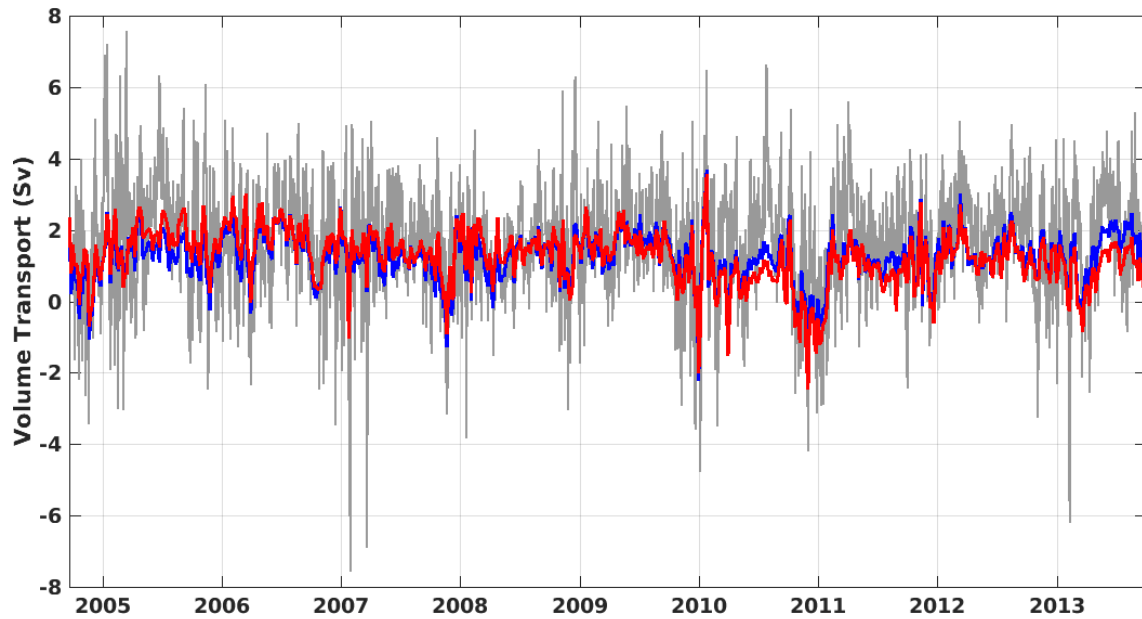
Figure 7. Volume flux through Davis Strait with HighRes (in red), LowResControl (in blue), and Davis Strait observations replotted from the mooring record discussed in Curry et al. (2014) (in grey). Positive values indicate southward volume fluxes through Davis Strait and negative values indicate the waters move northward.
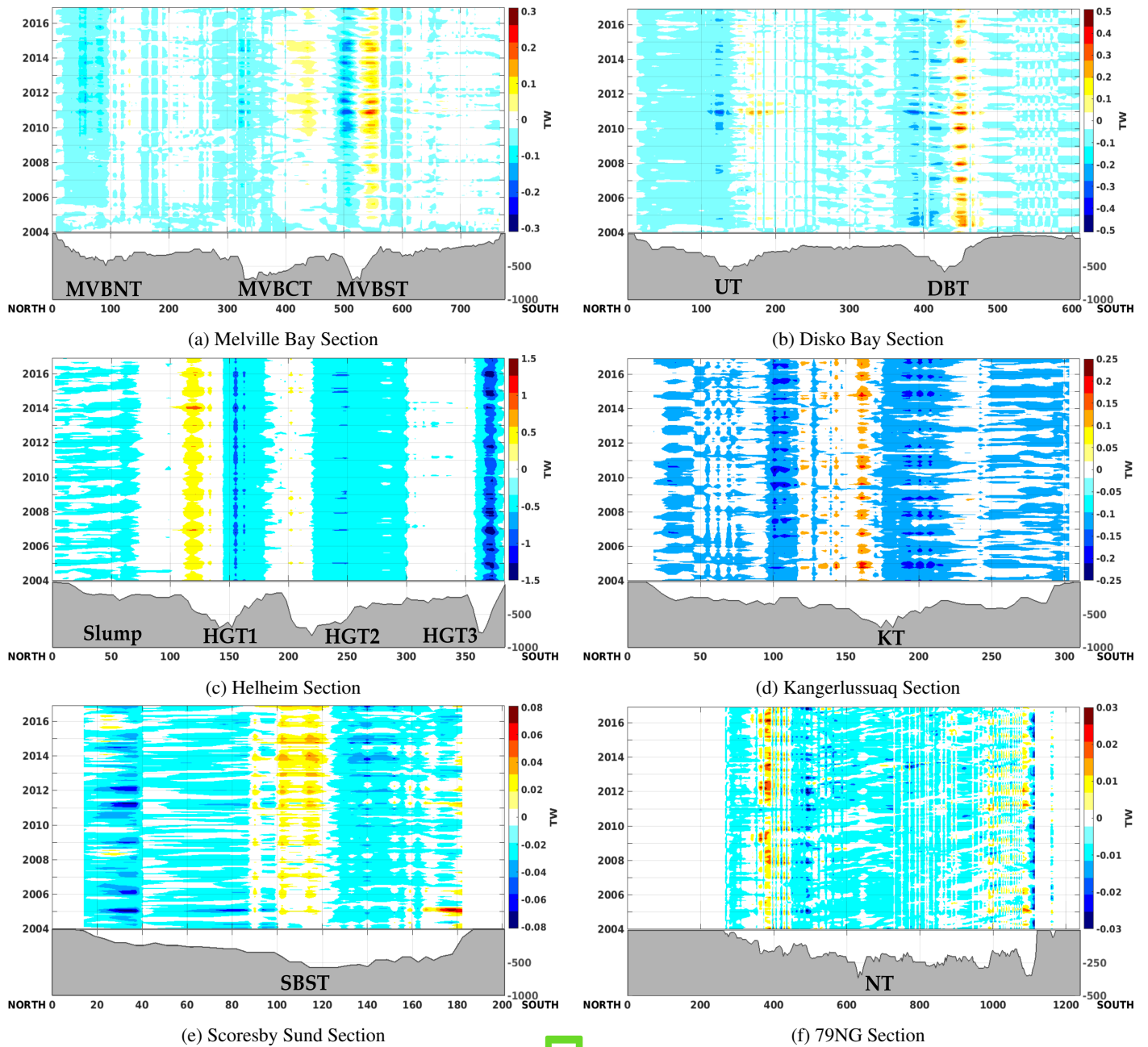
Figure 8. This figure shows the ocean heat exchange (flux) with respect to topography (in grey) within the time series of 2004 to the end of 2016 with the HighRes model output. These hovmoller plots show the monthly average heat flux coming on or off shelf in TW, (into or out of the page respectively), through a section (sections drawn in light purple on the map inset 1). Model bathymetry is in grey and the section runs north to south on the x-axis starting at the left hand side of the figure indicated by the zero kilometre marker. Along the y-axis is the depth for the bathymetry and then time for the 2004 to 2016 period. Colours indicate direction and magnitude of the on or off shelf heat flux (into and out of the page) and colourbar limits change per location .
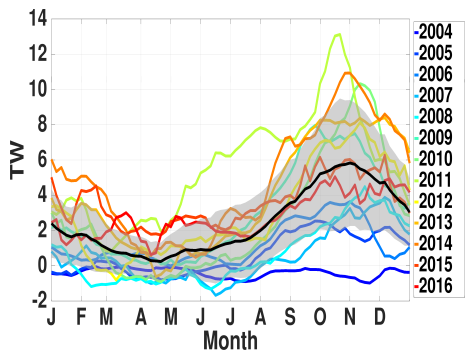
(a) Melville Bay Trough Heat Flux   (b) Volume Flux   (c) Average Temperature
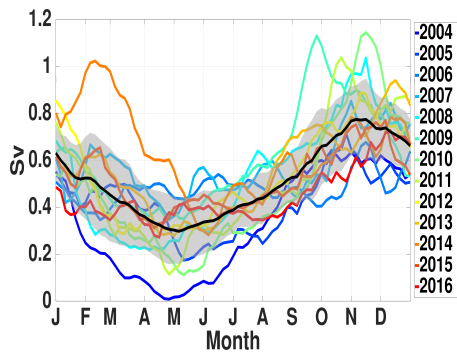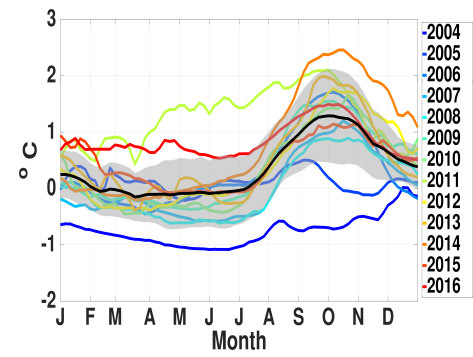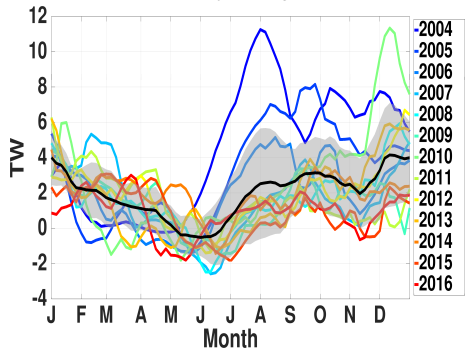
(d) Disko Bay Trough Heat Flux   (e) Volume Flux   (f) Average Temperature
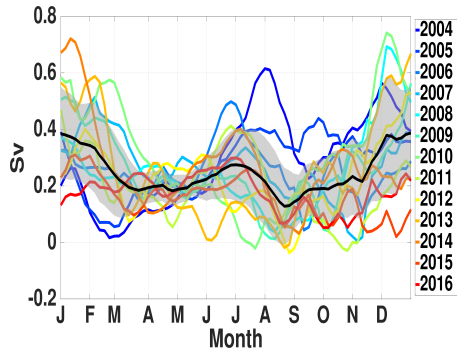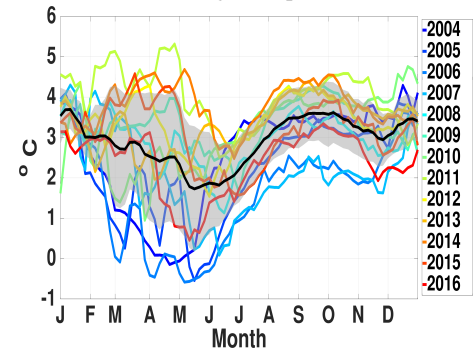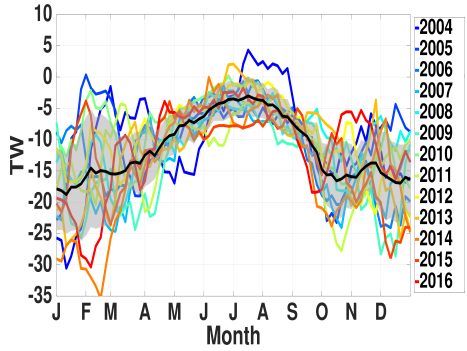
(g) Helheim Trough Heat Flux   (h) Volume Flux   (i) Average Temperature
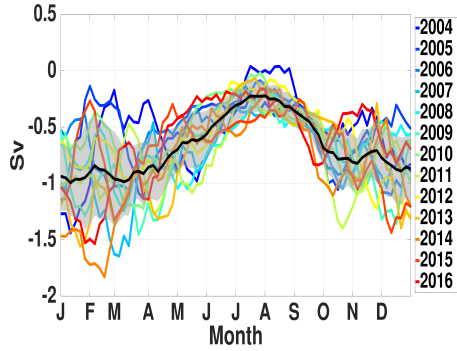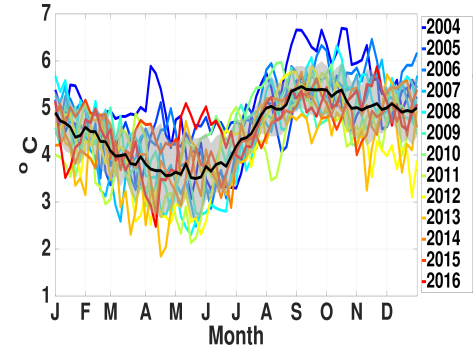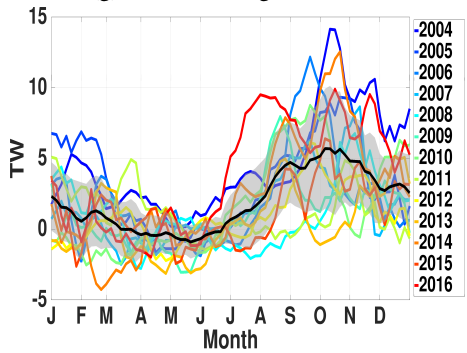
(j) Kangerdlussuaq Trough Heat Flux   (k) Volume Flux   (l) Average Temperature
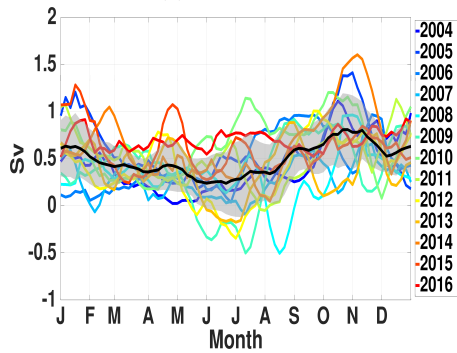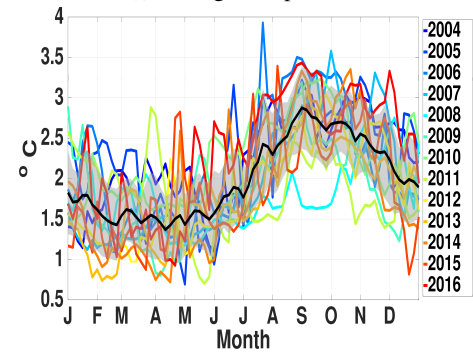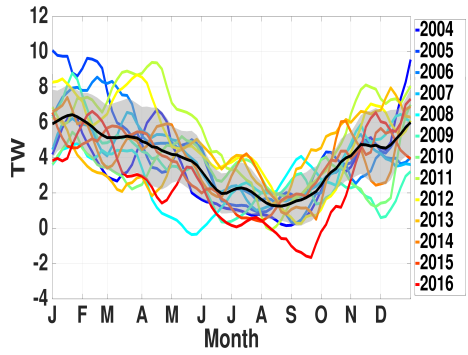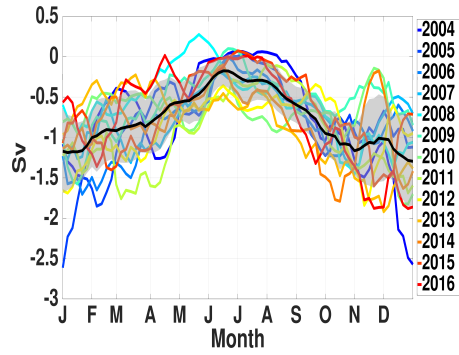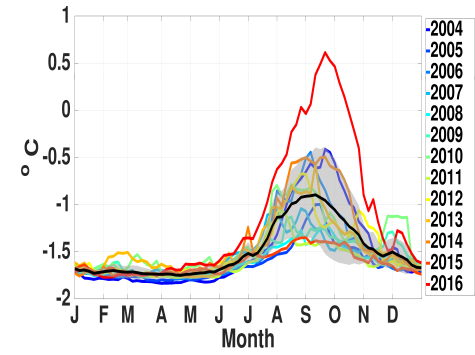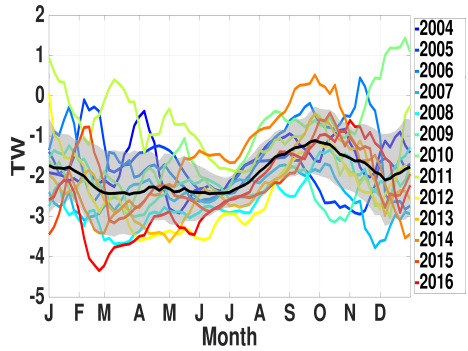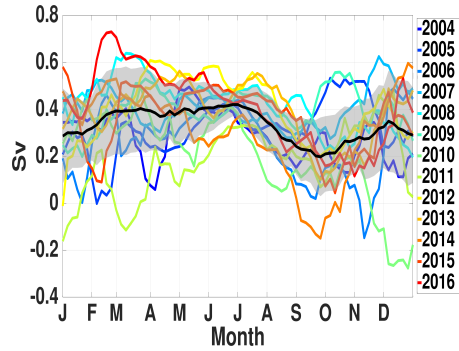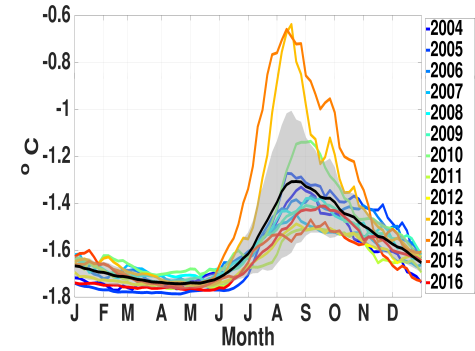
Figure 9. This figure shows the evolution and seasonality of the volume and heat flux, averaged over the entire depth, through each trough and average temperature across the section of the trough. The six locations are MVBCT, DBT, HGT2, KT, SBST, and NT (indicated in Fig. 1). The months are on the x–axis and the values of heat flux in TW, on the y–axis. The moving 25 day average heat flux for 2004 to 2016 (calculated using (Eq. 2)) is shown in black with one standard deviation window in grey. The years are indicated by colour, with earlier years starting in blue to later years in red.
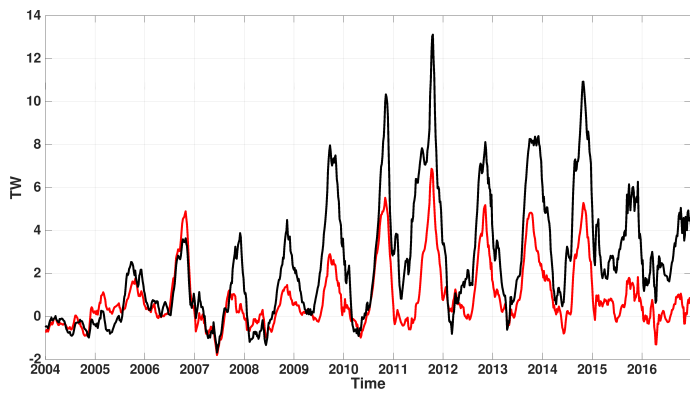
(a) MVBCT Mean
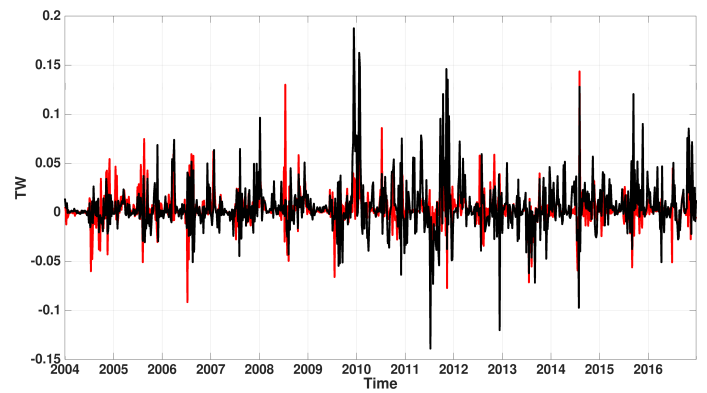
(b) MVBCT Fluctuation
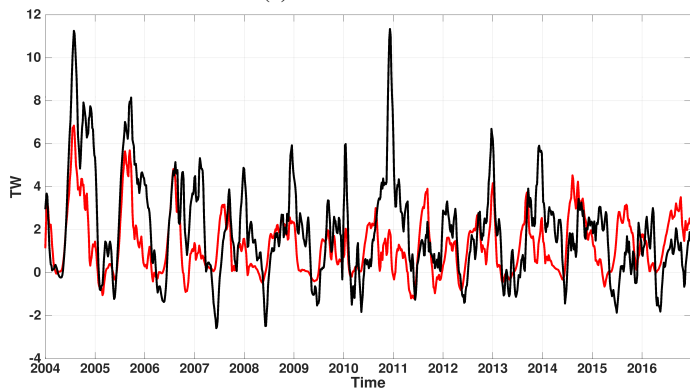
(c) DBT Mean
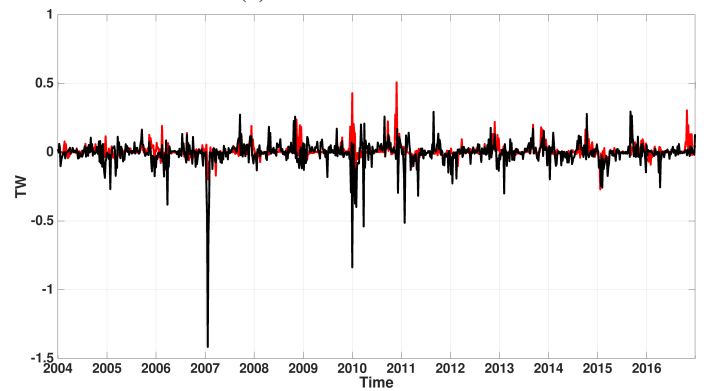
(d) DBT Fluctuation
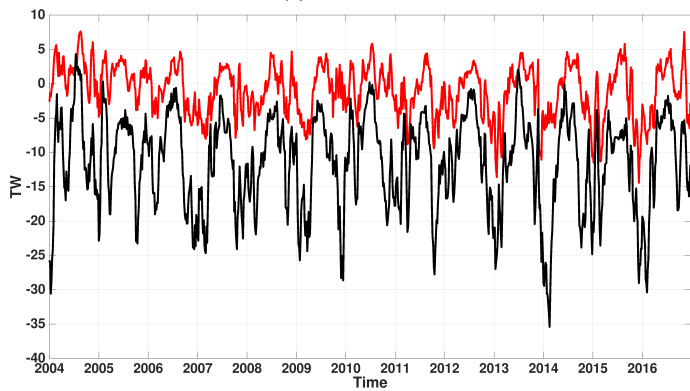
(e) HGT2 Mean
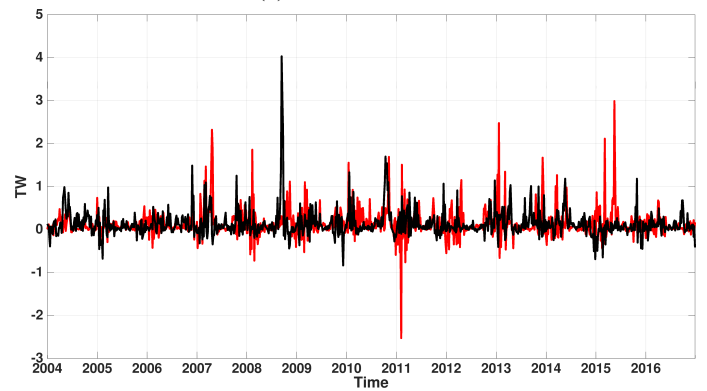
(f) HGT2 Fluctuation
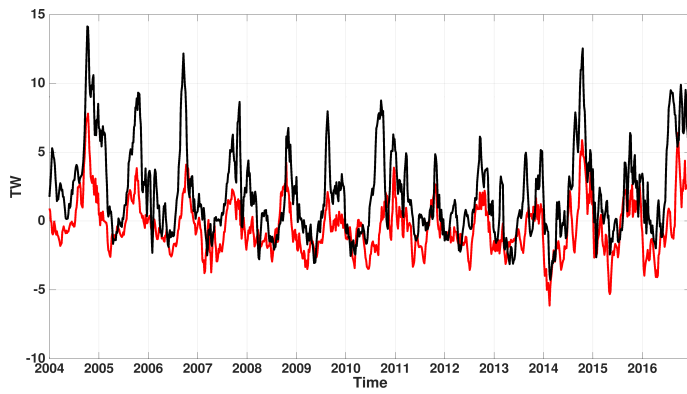
(g) KT Mean
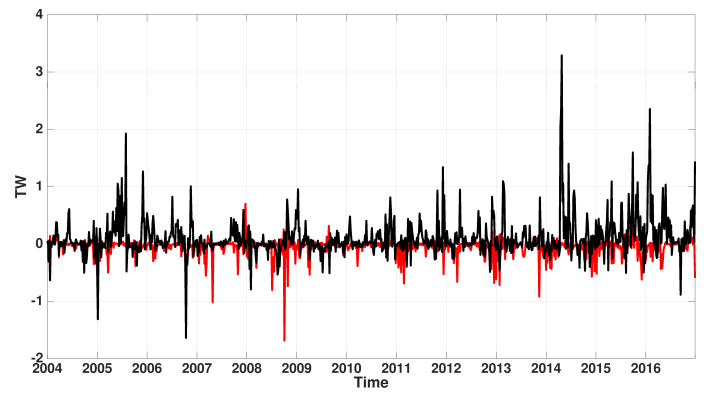
(h) KT Fluctuation
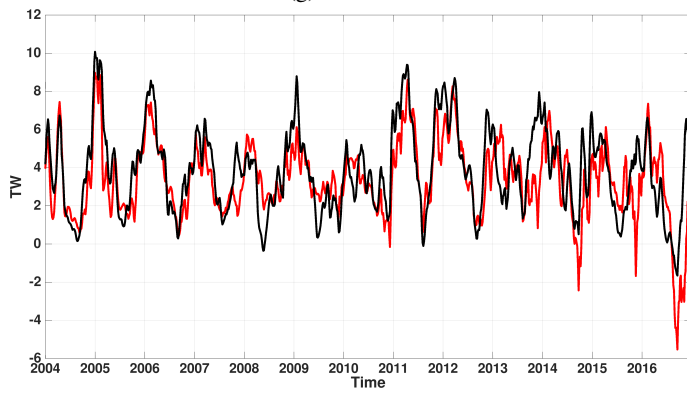
(i) SBST Mean
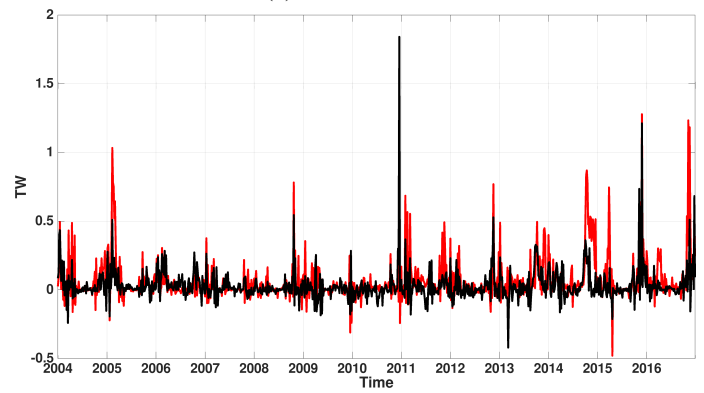
(j) SBST Fluctuation
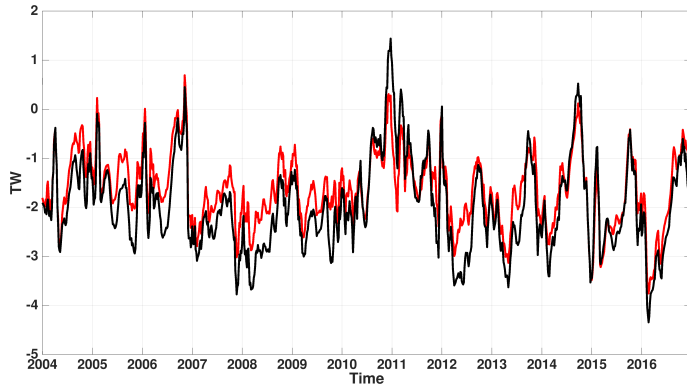
(k) NT Mean
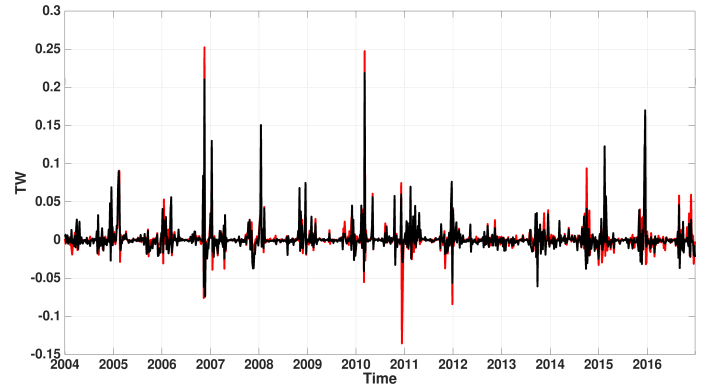
(l) NT Fluctuation
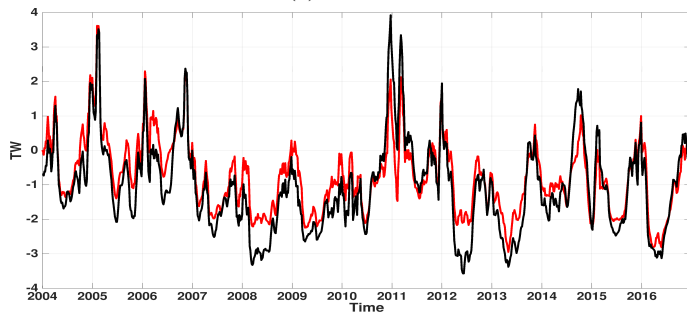
(m) NToff Mean
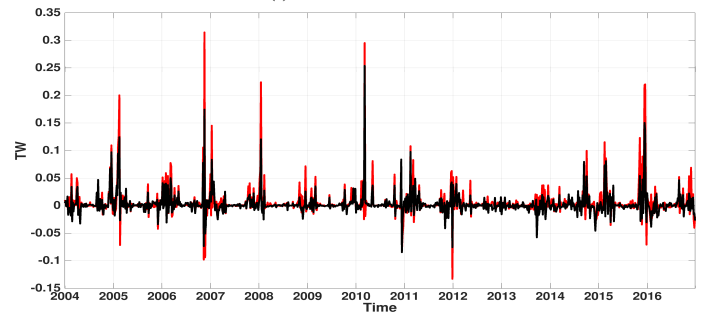
(n) NToff Fluctuation

Figure 10. This series of plots shows the heat flux comparison of two configurations, LowResControl (in red) and HighRes (in black). Mean flow on the left column and fluctuation of the flow on the right column. Plotted for the whole time series 2004 to 2016. Each row is for a different trough.
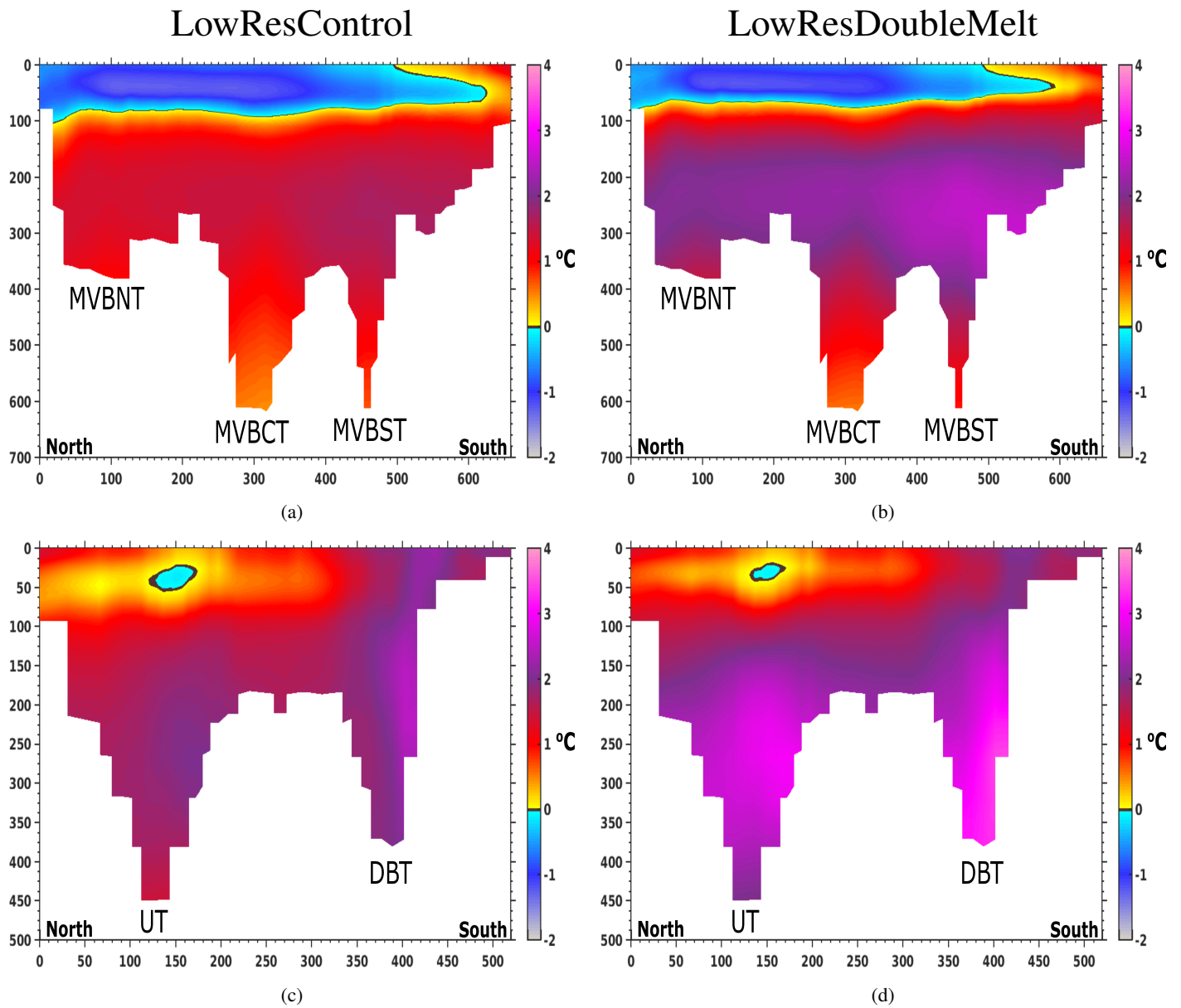
Figure 11. These figures show the temperature along two sections in the north-west of Greenland, Melville Bay Section and Disko Bay Section, for location the sections were drawn, see Fig. 1. This shows the average temperature from the period of 2004 to 2016, with the model bathymetry in white (m) and the colours indicate the temperature of the water in $^{\circ}C$. Left column shows the results for LowResControl, and the right column shows the results for LowResDoubleMelt. First row shows the section Melville Bay and the second row shows the section for Disko Bay.
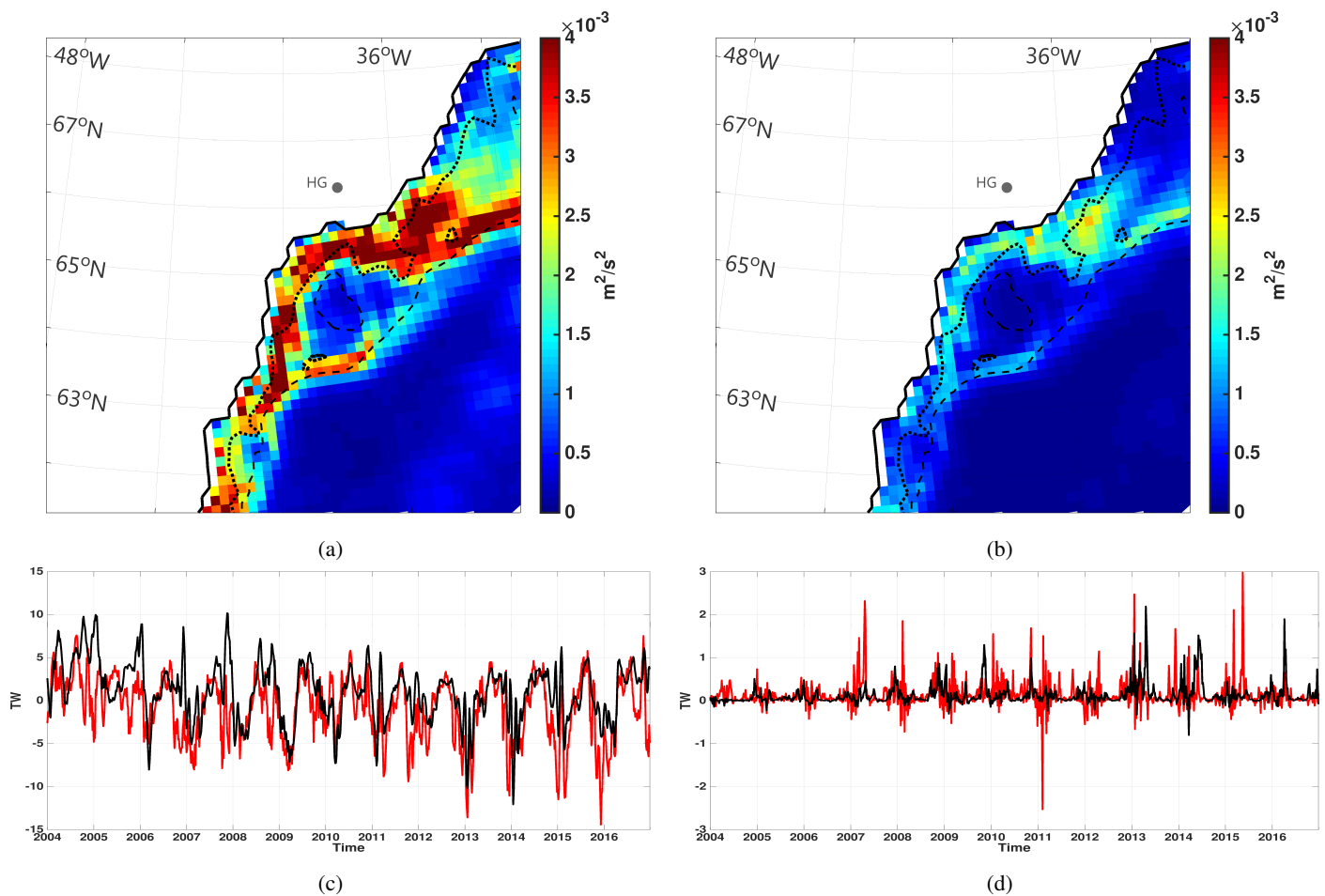
Figure 12. This figure shows how filtering the atmospheric forcing in LowResNoStorms, affects the turbluent areas. (a) and (b) shows the Eddy Kinetic Energy integrated over the entire depth at the south-east region of Greenland for LowResControl (a) and LowResNoStorms (b). The EKE here is the average EKE for the period of 2004 to 2016. The thick dashed lines mark the bathymetry at 250 m and the thin dashed line marks the 500 m depth. (c) shows the mean heat flux and (d) shows the fluctuation heat flux through Helheim Trough (HT) (location identified in Fig. 1). The LowResNoStorms configuration in black solid lines, LowResControl configuration in red solid lines.

Simulation	Resolution	Runoff	Atmospheric forcing
LowResControl	1/4°	50 % Greenland FWF	CGRF
HighRes	**1/12°**	50 % Greenland FWF	CGRF
LowResDoubleMelt	1/4°	**100 %** Greenland FWF	CGRF
LowResNoStorms	1/4°	50 % Greenland FWF	CGRF **Filtered** winds and temperature

Table 1. ANHA-NEMO simulations used in this study. All experiments include interannual river discharge from Dai et al. (2009) except the Greenland region, which is obtained by the Greenland Freshwater Flux (FWF) provided by Bamber et al. (2012). All simulations use the same atmospheric forcing, CGRF (Smith et al., 2014), but with the winds and temperature filtered in the LowResNoStorms.

Correlations of Heat Flux in Troughs Along the GrIS		
Trough	**Volume Flux with Heat Flux**	**Average Temperature with Heat Flux**
MVBCT	0.92	0.93
DBT	0.43	0.93
HGT	0.91	-0.25
KT	0.83	0.89
SBST	-0.73	-0.76
NT	-0.99	0.81

Table 2. Correlations of the averaged volume flux, heat flux and temperature for the entire timeseries (shown in the black line in Fig. 9) in troughs along the GrIS. The middle column shows the correlation between the volume flux and the heat flux and the column on the right shows the correlation between the average temperature across the section and the heat flux.

Troughs along the GrIS	Correlation between HighRes and LowResControl
MVBCT	0.84
DBT	0.54
HGT2	0.77
KT	0.71
SBST	0.74
NT	0.92
NToff	0.92

Table 3. This table shows the correlation of the total onshore heat flux summation of yearly heat (mean and fluctuation) fluxes from two configurations, HighRes, and LowResControl from 2004 to 2016. Troughs along the GrIS include Melville Bay Central Trough (MVBCT), Disko Bay Trough (DBT), Helheim Trough (HGT2), Kangerdlussuaq Trough (KT), Scoresby Sund Trough (SBST), Norske Trough (NT) and Norske Trough Off (NToff). These troughs can be identified in Fig. 1.

Troughs along the GrIS	Changes in onshore heat (%)
West Coast	
HighRes vs LowResControl	96%
LowResDoubleMelt vs LowResControl	37%
South-east Coast	
HighRes vs LowResControl	4%
LowResDoubleMelt vs LowResControl	-5%
North-east Coast	
HighRes vs LowResControl	9%
LowResDoubleMelt vs LowResControl	9%

Table 4. This table shows the percentage of the difference of the onshore sum of yearly heat fluxes from three configurations, HighRes, LowResControl, LowResDoubleMelt from 2004 to 2016. West coast includes Melville Bay Central Trough (MVBCT) and Disko Bay Trough (DBT), south-east coast sector includes Helheim Trough (HGT) and Kangerdlussuaq Trough (KT), and north-east coast includes Scoresby Sund Trough (SBST) and Norske Trough (NT). These troughs can be identified in Fig. 1.